Emergent Materials (2024) 7:443–472
https://doi.org/10.1007/s42247-024-00639-8

ORIGINAL ARTICLE

Assessment of fly ash and ceramic powder incorporated concrete with steam-treated recycled concrete aggregates prioritising nano-silica

Asha Uday Rao[1] · Prathibha P. Shetty[1] · Radhika Bhandary P[1] · Adithya Tantri[2] · Blesson S.[1] · Subhash C. Yaragal[3]

Received: 28 September 2023 / Accepted: 28 January 2024 / Published online: 21 February 2024

Abstract

Present research involves determining the effects of a proposed novel nano-silica prioritized-steam-treated recycled concrete aggregate (RCA) on microstructural, mechanical, and durability aspects of concrete incorporated with waste ceramic powder (WCP). The study on novel nano-silica prioritized-steam-treated recycled concrete aggregate revealed that 3% nano-silica induction with 3-h steam treatment for 50% adhered mortar bonded RCA performed optimally. The physical characterization of treated RCA showed improvement compared to untreated RCA, which was confirmed by microstructure study indicating the formation of additional calcium silicate hydrates in the bonded adhered mortar of treated RCA. Furthermore, as WCP has significant contents of alumina and silica, an optimum ternary binder mix was developed with cement, fly ash, and WCP. Later, a study was performed to analyse the performance of treated RCA incorporated in WCP prioritized concrete mix. The mechanical performance of WCP prioritized concrete with treated RCA was investigated through compressive strength, flexural strength, split tensile strength, and modulus of elasticity. The quality was ensured through ultrasonic pulse velocity, water absorption, and density characterization. The durability of concrete was studied with 5% concentrated hydrochloric acid attack and sea water (pH = 8.3 to 8.7) exposure conditions for a duration of 148 days (including 28 days of portable water curing period). Overall, 30% of the ternary mixture based on WCP prioritization, 50% adhere mortar-based RCA, and 3% of nano-silica prioritization steam treatment (3 h) demonstrated the best performance in terms of both mechanical and durability aspects. The study concluded that due to its improved performance, the innovative nano-silica priority steam treatment approach could replace 100% of RCA in concrete. Furthermore, treated RCA being advantageous because of easy adoptable technique for real-time practices as well as maintaining consistency regards RCA characteristics throughout concrete mixture be the challenge.

✉ Adithya Tantri
tantri.adithya@manipal.edu

Asha Uday Rao
asha.prabhu@manipal.edu

Prathibha P. Shetty
pp.shetty@manipal.edu

Radhika Bhandary P
radhika.st@manipal.edu

Blesson S.
blesson.s@learner.manipal.edu

Subhash C. Yaragal
subhashyaragal@nitk.edu.in

[1] Department of Civil Engineering, Manipal Institute of Technology, Manipal Academy of Higher Education, Manipal, Karnataka 576104, India

[2] Department of Civil Engineering, Manipal Institute of Technology Bengaluru, Manipal Academy of Higher Education, Manipal, Karnataka 576104, India

[3] Department of Civil Engineering, National Institute of Technology Karnataka, Surathkal, Mangalore 575025, India

1 Introduction

Worldwide production and consumption of ceramic tiles reached 18,339 million m^2 as of 2022, a rise of 7.2% from 2021 [1]. Every year, India produces more than 100 million tonnes of ceramic goods [2]. It has been the origin of 16 to 30% of the ceramic trash produced [3]. Additionally, as ceramic waste is robust, resistant to forces of physical degradation, and being highly resistant to chemical, biological, and physical deterioration, its waste disposal has proven to be challenge [4, 5]. Particularly, the dried ceramic waste powder is dangerous to environment. Utilising ceramic waste powder as a value-added ingredient that acts as a secondary binder material after cement has provided a chance to overcome these problems. Following a series of experiments, it has been concluded that there are no negative impacts on the mechanical behaviour of cement when up to 30% of ordinary Portland cement (OPC) is substituted with waste ceramic powder [6–11]. However, at the same time as when they are being integrated in concrete, ceramic wastes cause poor rheological qualities in concrete by increasing friction due to specific surface area discrepancies [10, 10, 12]. Ceramic tiles typically have a glossy surface on one side and a clayey texture on the other, which accounts for the varying surface area or textural inconsistencies [5, 13, 14]. Despite the fact that its inclusion reduced the specific gravity, which leading to lightweight concrete, there was an increase in water absorption [14–16].

Chemical characteristics of ceramics showed the presence of silica, which ranges from 29.1 to 71.89% as the primary rich content, alumina, which ranges from 7.3 to 24.46% as the secondary rich content, and ferric oxide, which ranges from 0.5 to 7.7% as the tertiary rich content. This chemical composition is the reason to use ceramic waste powder as pozzolanic material and has been responsible for improvement in strength parameter of concrete [7, 7, 11, 17–22]. According to Nair et al. [23], the presence of SiO_2 and Al_2O_3 contents improves the reaction degree while reacts with Ca $(OH)_2$ of cement resulting in the formation of greater (> 60%) CSH and CAH gels. However, the percentages of silica, alumina, and ferric oxide that vary from source to source are determined to be 42.79%, 17.16%, and 7.2%, respectively, which indicates that chemical properties are not uniform [24, 25]. The causes for these variations include the white ceramics (rich in silica) that are supplementary wastes of sanitary ware, white stoneware tile, and porous stone ware tiles, followed by the red ceramics (rich in alumina) that are extra wastes of bricks, stoneware, and roof tiles [24–26]. Due to latter stage reactivity properties of rich alumina, the rheological properties of cement are improved when red ceramic waste powder is used [11, 24, 25]. However, because of the higher reaction time of rich silica, the rheology qualities of cement restrict the use of white ceramic waste as a secondary binder [24, 25]. Furthermore, the higher durability properties are contributed by ceramic waste powder due to the presence of crystalline aluminosilicate [27]. Particularly, ceramic powder outperforms other materials under acid and sulphate attack. It was discovered that adding 30% ceramic waste to concrete helped it withstand sulphate attack and acid attack while only losing 5 to 15% of its compression strength properties compared to conventional concrete, which lost about 25% more [24, 28]. In general, when ceramic waste powder is mixed with cement as a secondary binder material, the oxide variation and chemical compositional non-uniformity promote research opportunities to understand and analyse the rheological and mechanical properties of the powder. Furthermore, research on the literature reveals that the effectiveness of ceramic waste powder exposed to seawater has not yet been examined in terms of durability which is one of the objectives of the present study.

Recycled concrete aggregate adoption in concrete has become common in recent studies as the second major component of concrete or what might be considered the skeleton of concrete [29–31]. Recent studies indicate recycled concrete aggregate-based concrete performance is inferior to those of regular concrete [32, 33]. Poor characteristics of adhere mortar covering the recycled concrete aggregate being the predominant factor for inferior performance, researchers have focused on either partially reducing or removing the adhere mortar. Tantri et al. [34] placed freezing–thawing-conditioned recycled concrete aggregate in abrasion chamber in Los Angeles and were successful in removing more than 75% of adhered mortar. As a result, recycled concrete aggregate's water absorption properties decreased by about 2.36%, but the aggregate's toughness properties were compromised. In the act of second concept, researchers discovered an alternative approach to strengthening adhered mortar of recycled aggregate that uses blended fibres, carbonation, chemical treatment, and mineral admixtures [35–40].

The first idea was to give the external mortar a greater support by employing mixed fibre and mineral admixture [41, 42]. To increase the mechanical and toughness properties of RCA, Cakir [43] specifically suggested an ideal ratio which is use of 50% recycled concrete aggregate with 5 to 10% of silica fume as a mineral additive. In the other context, strengthening the adhered mortar through chemical treatment, acetic acid was used as chemical admixture, and it was discovered that by submerging recycled concrete aggregate in it and applying pressure, it was possible to strengthen ITZs in greater aspects while also improving the durability of concrete as reported by Kazmi et al. [44, 45]. Current

research employs a chemical treatment based on nano-silica to reinforce interface transition zones (ITZs) and fill in minuscule microgaps in adhering mortar, resulting in a 7 to 12% decrease in the water absorption properties of concrete [39, 46]. Furthermore, Sing et al. [47] found that treating of recycled concrete aggregate with nano-silica increased the specific gravity by 18%, which improved the aggregates' mechanical qualities. Overall, there has not been significant research done on the chemical treatment of recycled aggregate using nano-silica. In particular, there has not been investigated on the novel chemical treatment that involves soaking recycled concrete aggregate in a nano-silica solution and then treating it with steam.

Concrete's durability can be defined as its capacity to withstand abrasion, chemical attack, and weathering while retaining the desired engineering qualities [28, 48, 49]. Depending on the exposure environment and intended qualities, different concretes require varying levels of durability. The two most potent natural danger concrete structures near the shore are hydrochloric acid (HCl) and sea water (alkaline attack) [9, 50]. On the first account, exposure to HCl results from urban activity, although they typically come from industrial processes [51] and are found in significant amounts in sewage systems as well. The processes of decomposition and leaching of cement paste components are impacted by acidic attack [52]. Many studies revealed that while concrete is exposed to HCl (5% concentration), mechanical properties of concrete reduced in the range of 16 to 68% depending on the nature of the acid used [53]. Concrete becomes substantially more porous when exposed to acidic liquid and in fact, it was found that concrete exposed to HCl had a critical loss happening in ITZ which roughly accounted for seven to ten times higher loss than the concrete stored in a sanitary environment [54].

Further on the account of second potent danger near shores, the specifications for concrete exposed to tidal seawater will differ from those for a concrete floor inside. Generally, sea water consists of 3.5% of soluble salts by weight, having Na^+ and Cl^- in highest ionic concentrations (11,000 and 20,000 mg/l, respectively) [55]. Nonetheless, enough Mg^{2+} and SO_4 are present typically 1400 and 2700 mg/l, respectively to take an aggressive approach to cement concrete. The pH of saltwater ranges from 7.5 to 8.4, with an average pH of 8.2 being in equilibrium with atmospheric CO_2 which has been the representative of alkaline attack on concrete [56, 57]. Many discoveries revealed that when concrete is exposed to sea water, the presence of excessive salt improves infiltration, which causes deterioration, but the use of finer materials with OPC, such as fly ash, epoxy, and silica fumes, restricts the infiltration by reducing the concrete pores and makes it possible to reduce deterioration in concrete by 5 to 30% [58–61]. However, Shi et al. [50] discovered that exposure to sea water improved the mechanical properties of a metakaolin-based concrete mixture by producing Friedel's salt in the concrete, which improved the connection between average pore diameter and compressive strength. These pros and drawbacks provide the opportunity to study the importance of concrete's mechanical and microstructural components when exposed to seawater. Furthermore, the durability of concrete constructed with nano-silica-treated recycled aggregates under seawater exposure has not been the subject of any research studies until today. Overall main objective of the proposed study is to develop sustainable novel treated recycled aggregate incorporated concrete.

2 Material details

2.1 Binder materials

In the present study as the part of the traditional practice, ordinary Portland cement (OPC) is the primary binder which confirms to the specification requirement of IS 4031 (Part 6) [62], followed by class F fly ash (FFA) as secondary and waste ceramic powder (WCP) as tertiary binders. Nano-silica (NS) treatment powder is used to prepare treatment solution for RCA. Table 1 represents the physical and chemical characteristics of binder materials. It is seen from Table 1 that among the binders used, OPC has the highest specific gravity followed by FFA, WCP, and NS respectively. But the specific surface area of NS is found to be as high as expected which confirms more interface while binds with other constituents of proposed mixture as well as it helpful for acceleration of chemical reaction. While comparing OPC, FFA, and WCP with respect to specific surface area, it is observed that WCP has 120.39% higher specific surface area than FFA and is followed by OPC. Figure 1 represents 3D ternary plot of chemical characteristics of all binders which confirms their pozzolanic characteristics, specifically NS found to be prioritized as a pozzolana followed by WCP and FFA. As expected, OPC alone represents cementitious property. Figure 2 represents particle diameter distribution pattern of binders, wherein D_{10} and D_{50} of OPC and FFA are found to be similar, but at D_{90}, a significant difference of about 11.27 µm between FFA and OPC is observed. WCP is found to be much finer by representing D_{mean} of about 6.72 µm followed by FFA and OPC. But overall NS is found to be much finer than all other binder materials representing D_{mean} of about 16.4 nm. Figure 3 presents microstructural and element identification of binders, which reveals the presence of irregular and angular shaped crystals with regard to WCP followed by OPC and NS. It is also confirming presence of Si, Al, and O ions in WCP, Ca, K, O, Na, Mg, Al, Si, and S ions in OPC and Si, Ti, C, K, Ca, Fe, Na, O, and Al ions in FFA. Specifically, Si and Al are necessary to initiate pozzolanic activity which is present in all binders. In addition to this, Si ions are identified as the highest peak in NS.

Table 1 Physical and chemical properties of dry state binders

Physical properties of binder agents				
Properties	NS	WCP	FFA	OPC
Specific gravity	2.31	2.61	3.09	3.12
Specific surface area (m^2/kg)	201,000	555	461	349
Fineness (%)	-	5.44	4.55	3.51
Diameter of binder at 10% of cumulative passing (D_{10})	2.2 (nm)	1.53 (μm)	2.66 (μm)	2.91 (μm)
Diameter of binder at 50% of cumulative passing (D_{50})	11 (nm)	6.01 (μm)	15.07 (μm)	15.68 (μm)
Diameter of binder at 10% of cumulative passing (D_{90})	36 (nm)	13.10 (μm)	29.10 (μm)	70.94 (μm)
Mean diameter (Mean "*D*")	16.4 (nm)	6.72 (μm)	15.53 (μm)	26.80 (μm)
Chemical composition of binder agents				
Cao	-	0.50	3.56	63.15
SiO_2	99.81	47.00	30.43	21.20
Al_2O_3	0.02	37.00	8.31	6.20
Fe_2O_3	0.003	1.00	36.63	4.75
MgO	-	0.50	5.39	1.60
K_2O	-	2.18	5.64	1.00
Na_2O	-	0.65	0.03	0.30
SO_3	-	0.10	0.03	1.45
LOI	-	43.60	2.52	1.3

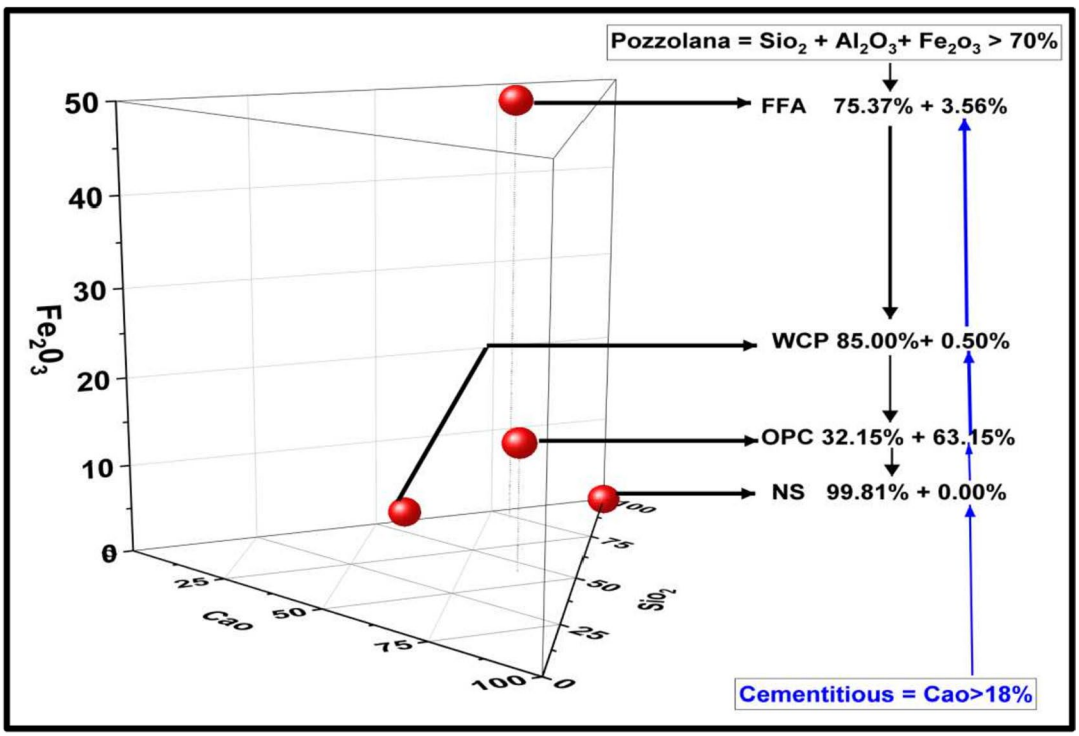

Fig. 1 3D ternary plot of dry state binders

Fig. 2 Particle diameter chart

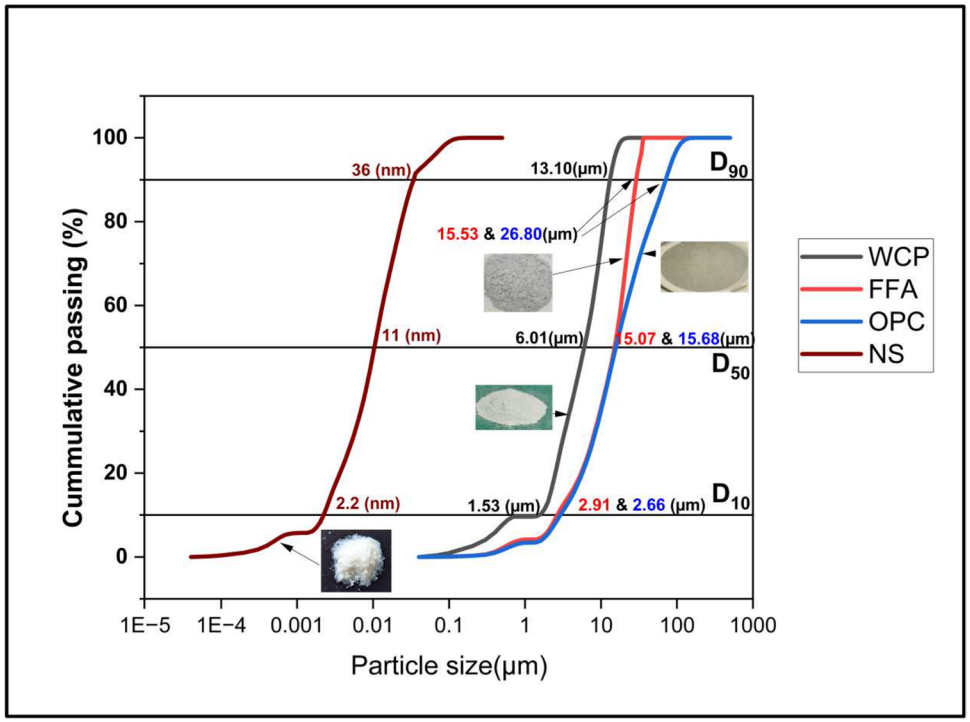

2.2 Recycled concrete aggregates and PQD sand

Concrete cubes that were tested in the laboratory and discarded as waste were crushed to produce the recycled aggregates for concrete. To get rid of all the dust and fine aggregates that were present in the crushed aggregates were sieved and cleaned. To get rid of the moisture, the material was further sun-dried. Figure 4 displays the final RCA aggregates along with the gradation pattern. To describe the material characteristics of the recycled aggregates, a variety of tests have been carried out and the outcomes of the material's qualities are presented in Table 2. The average specific gravity value was calculated to be between 2.51 and 2.61, which is well within the parameters. According to IS 383:2016, natural aggregates can absorb between 0.1 and 2% of water, while the maximum water absorption rate for recycled aggregates according to IS 383:2016 [63] is 5%. According to IS 383:2016 [63], recycled aggregate and recycled concrete aggregate may have higher water absorption rates of up to 10%, when subject to pre-wetting (saturation) of aggregates prior to batching and mixing. According to IS 2386 Part 4 (1963) [64], the aggregate impact value for wearable surfaces, such as runways, should not exceed 30%, while the value should not exceed 45% for non-wearable surfaces. The impact value obtained for RCA used in the present study indicates that it can be utilized for structural purposes in concrete. As per IS 2386 Part 4 (1963) [64], for wearable surfaces like runway, the LA abrasion value should not exceed 30% and for non-wearable surface, the value should not exceed 50%. The observed LA abrasion value presented in Table 2 indicates the suitability for use in concrete as in structural purpose but not suitable for wearable surfaces. As per IS 2386 Part 4 (1963) [64], aggregates with crushing value greater than 30% are considered anomalous. The above properties discussed thus indicate that the sample of RCA used for the study is partially suitable for direct use in concrete, whereas some properties such as water absorption and crushing value indicate that these RCA samples are much inferior compared to the permissible values as per IS codes. Hence, in this study, attempt has been made to improve the property of these RCA by novel nano-silica prioritized steam treatment.

In addition to this, fine aggregate used in the current investigation is processed quarry dust (PQD) sand obtained from granite quarry nearby Manipal, Karnataka, India. Reason been for the choose of PQD sand is scarcity of river sand or natural sand as well as it promotes sustainability aspects as well. The PQD sand is cubical in shape with grounded edges and is graded as a building material after being cleaned. PQD sand is available in sizes ranging from 4.75 mm to 150 microns and Fig. 4 displays the particle size distribution of PQD sand. PQD sand complies with IS 383:1970 Zone II.

2.3 Novel treatment procedure of recycled concrete aggregate

The treatment procedure for RCA involves four stages: the first stage is to understand relation between old, adhered mortar percentages, which is determined based on the

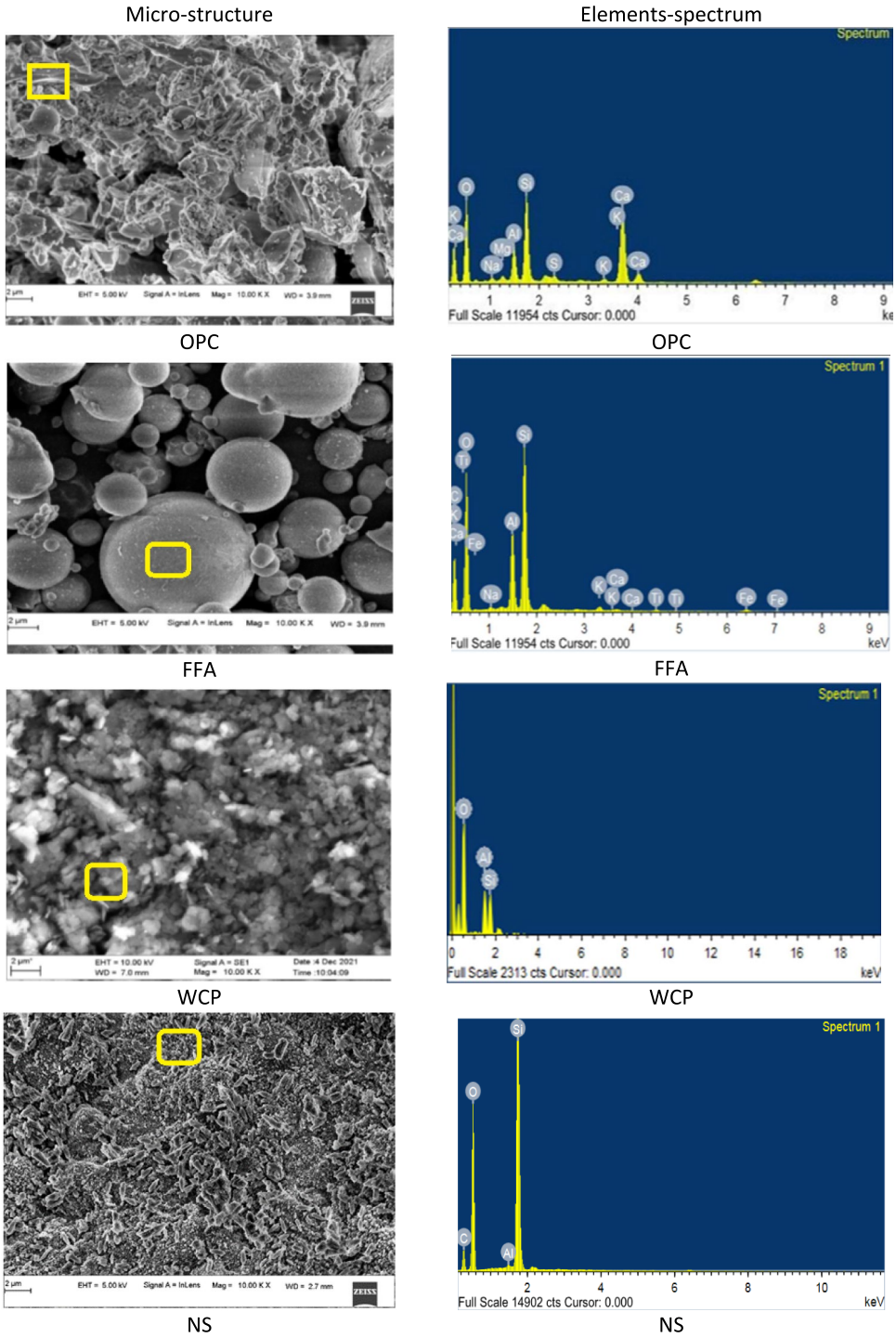

Fig. 3 Microstructural with EDS locations and elements-spectrum chart

number of rotations offered in the Los Angeles abrasion testing machine. The sample with 500 rotations on the abrasion machine is considered to have almost 0% old, adhered mortar. Furthermore, the number of rotations required to attain 75%, 50%, and 25% of adhered mortar is determined by trial-and-error process as presented in Table 3.

The second stage of treatment procedure is the preparation of nano-silica solution, which is prepared by slowly suspending the nano-silica over the surface of water and continuously stirring the solution with the help of a standard 100 RPM motorized mixing arrangements. Care is taken to make sure that the nano-silica added does not form lumps and settle in the bottom. The concentration of nano-silica is

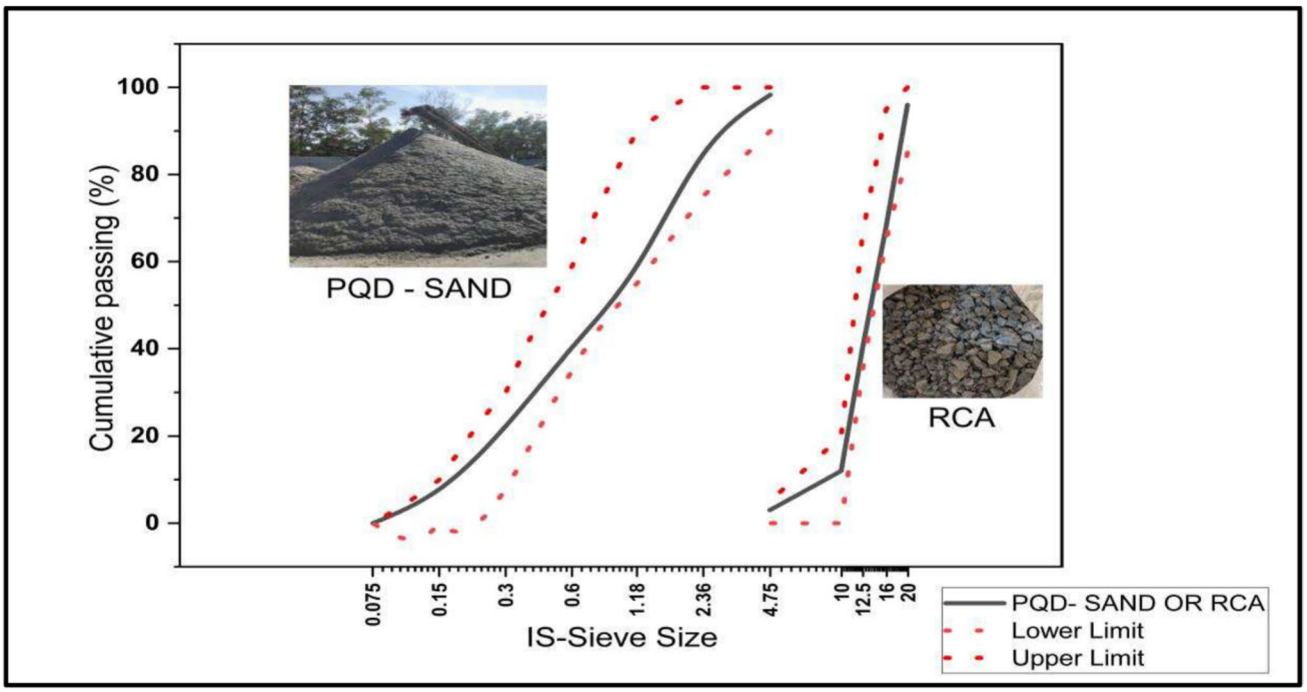

Fig. 4 Particle size distribution of aggregates

Table 2 Physical properties of dry state aggregates

Properties	RCA	PQD sand
Specific gravity	2.51	2.61
Water absorption (%)	5.04	1.12
Impact value (%)	32.07	-
Abrasion value (%)	42.27	-
Crushing value (%)	34.65	-

Table 3 Physical properties of dry state aggregates and its designations

No. of rotations on the abrasion machine	Considered percent of old adhered mortar	Designation of mixes of nano-silica (3%)-treated RCA
0	75%	75-NS3-TRCA
45	50%	50-NS3-TRCA
125	25%	25-NS3-TRCA
500	0%	0-NS3-TRCA

For untreated RCA, it represents as "UTRCA", for example 75-UTRCA, 0-UTRCA; *NS3*-Nano-Silica (3%)

defined as the percentage by weight of nano-silica to weight of water. The percentage of nano-silica varies from 0.5 to 4% by the weight of water.

The third stage of treatment procedure involves soaking of RCA in prepared nano-silica solution for 24 h under room temperature. Prior to soaking of RCA, they are washed, oven dried to remove all the water present in them, and cooled to room temperature. During this soaking stage, water acts as the transmitting agent for nano-silica to get into adhered mortar pores and helps to initiate pozzolanic reaction.

Finally, in the fourth stage of treatment procedure, the nano-silica-infused RCA are subjected to steam curing at an elevated temperature of about 100 °C for 3- and 6-h duration. During this stage, an accelerated pozzolanic reaction occurs where in unreacted cement present in adhered mortar reacts with nano-silica at elevated temperature, which converts silica-rich predecessor with no cementing properties to calcium silicate having good cementing properties. There is a pozzolanic reaction between calcium hydroxide known as portlandite and silica acid ($Ca(OH)_2 + H_4SiO_4 \rightarrow CaH_2SiO_4.2H_2O$; $CH + SH \rightarrow C - S - H$). Furthermore, soon after the steam curing, the RCA are removed and placed for sun drying for the removal of moisture content in it and stored it with airtight arrangements.

To standardize this novel treatment procedure, performance of treated RCA is evaluated with respect to crushing strength characteristics of RCA aggregates which is presented in Fig. 5. It is found that 3% NS with 3-h steam curing demonstrates optimal behaviour with regard to increase in crushing strength of aggregates, and by maintaining negligible difference with 4% NS treatment. The reason may be the surface interaction limitation of adhered mortar texture [46, 65–67]. It is therefore confirmed that for RCA, a 3%

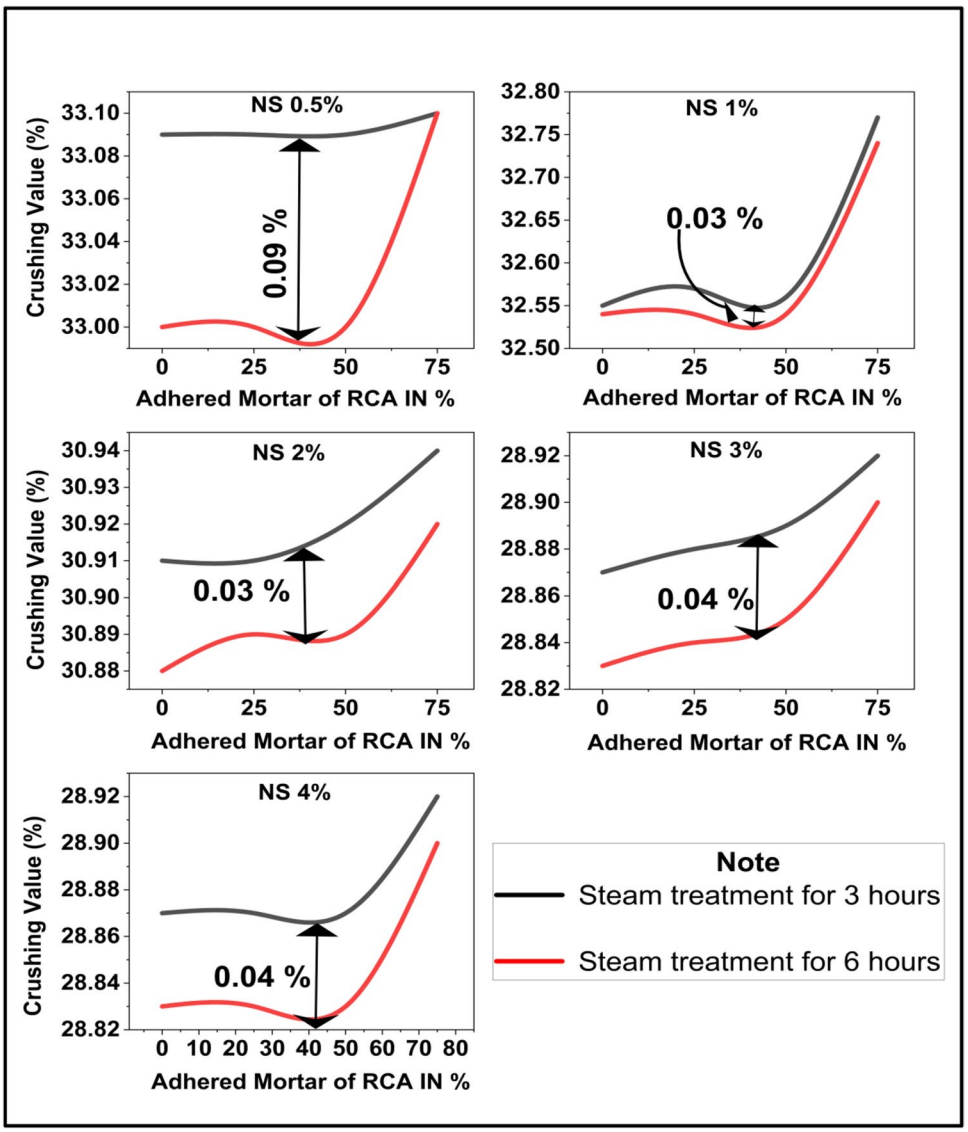

Fig. 5 Treated RCA performance

NS solution soaking with 3-h steam curing at 100 °C is the standardized treatment procedure for improvement in its performance.

2.4 Treated Recycled Concrete Aggregate (TRCA) characterization

As mentioned before (refer to Section 2.3), 3% nano-silica (NS) with 3-h steam treatment been standardized for all RCA variants contains difference adhered mortar percentages and mix notations as mentioned in Table 3. Physical characterization of these aggregates has been evaluated through crushing strength (presented in Fig. 5), Los Angles abrasion test, impact test, and water absorption test. Figure 6 represents that 50-NS3-TRCA found to be optimum performed aggregate followed by 75-NS3-TRCA, 25-NS3-TRCA, and 0-NS3-TRCA. 50-NS3-TRCA represents 9.74% decrement in water absorption, 3% increment in impact value, 2.5% increment in abrasion value, and 20.5% increment in crushing strength when compared to 50-UTRCA. The reason being denser characterization of 50% adhered mortar due accelerated pozzolanic reactivity achieved while exposure to NS prioritized steam treatment.

Furthermore, this has been confirmed through chemical characterization and microstructure analysis of treated adhered mortar of RCA which are evaluated through XRD and FE-SEM. FE-SEM was performed on Oxford Instrument Carl Zeiss FESEM with 200 nano-metre (nm) scale followed by 10kv EHT, 40.00 KX magnification; considered width is 7 to 9.5 mm. Furthermore, XRD was performed utilising a Rigaku Mini-flex 600 with a broad-angle detection of 10–90° 2θ value, to investigate spectroscopy stages of treated RCA. Figure 7 represents the XRD characterization of treated and untreated RCA, and there is

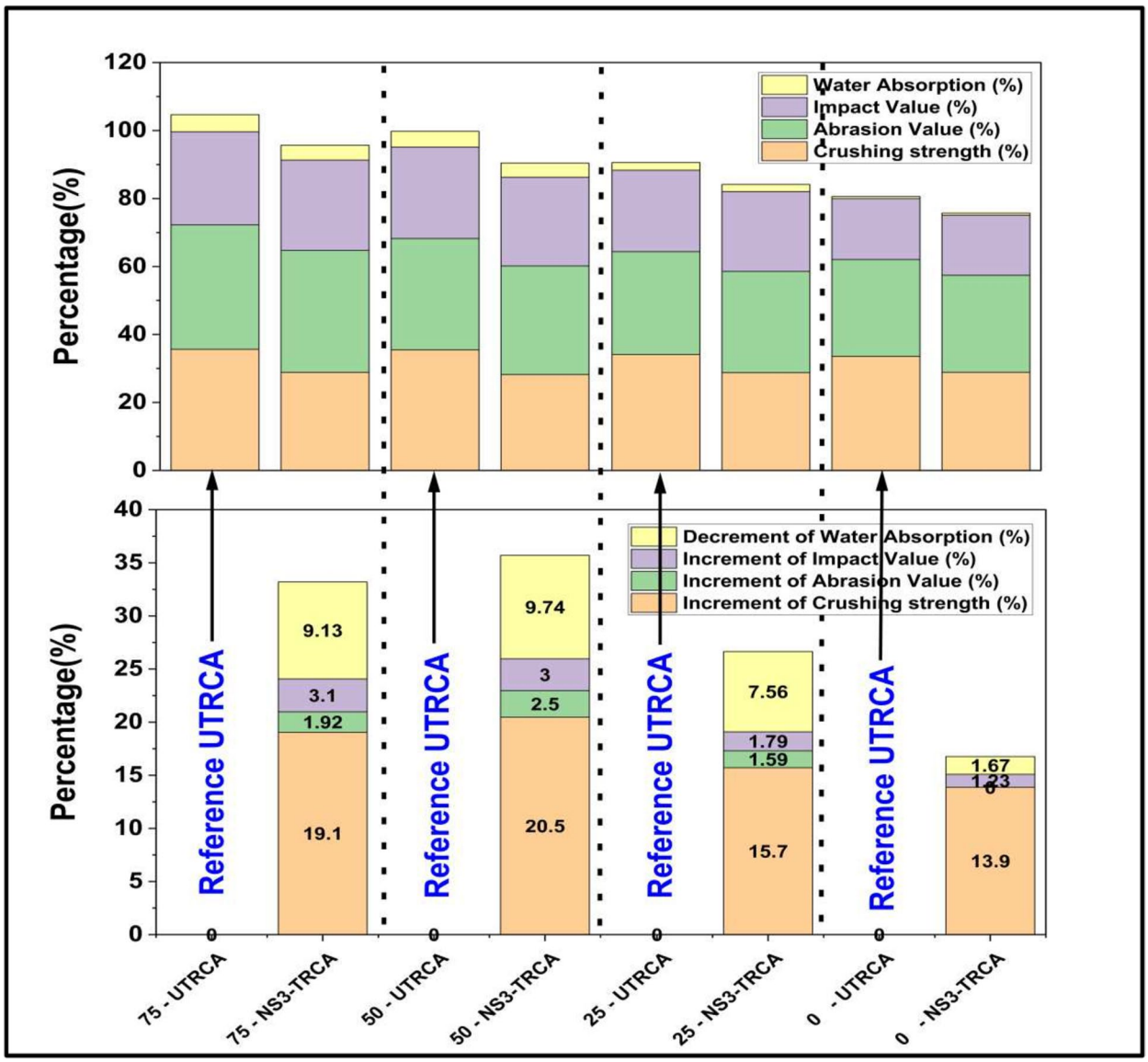

Fig. 6 Physical characterization of NS-treated TRCA and UTRCA. [Note: Example for elaborate form of mix "50-NS3-TRCA" is expressed as 50 be the adhered mortar percentage; NS3 is nano-silica 3%; TRCA means treated recycled concrete aggregate; UTRCA means untreated recycled concrete aggregate]

significant formation of additional CSH crystals in TRCA as compared to UTRCA. Specifically, for 50-NS3-TRCA, quantified CSH found is 40.4% which has been the highest, followed by 39.4% for 75-NC3-TRCA, 37% for 25-NC3-TRCA, and 35.6% for 0-NC3-TRCA. Table 4 confirms the identification of CSH in the form of clinotobermorite, CH in the form of portlandite, ettringite, and CC in the form of calcite. These identifications are specific validation for the increased crushing resistance and improved physical characteristics of 50-NS3-TRCA aggregates. Figure 8 represents FE-SEM nano-metre scaled images and it reveals the presence of agglomerates in UTRCA and formation of new CSH, CC, CH, and E in TRCA. These findings from FE-SEM confirm and are in line with the physical characteristics and XRD findings of TRCA. Energy-dispersive spectroscopy (EDS) was performed on TRCA, and the identified elements revealed the atomic % of Si, Al, and Ca which are found to be major for all TRCA as presented in Table 5. Specifically, as expected, Si was found to be the primer. Si, Al, Ca, Si + Al, Ca/(Si + Al), and Ca/Si are found to be incremental as the increase of adhered mortar content in TRCA from zero and up to 50%. This increase may be due to the sufficient exposure through intercontact area of adhered mortar followed by sufficient porous connectivity (as observed for UTRCA in Fig. 8) which helps with contact to NS solutions although Si/Al and Ca/Al

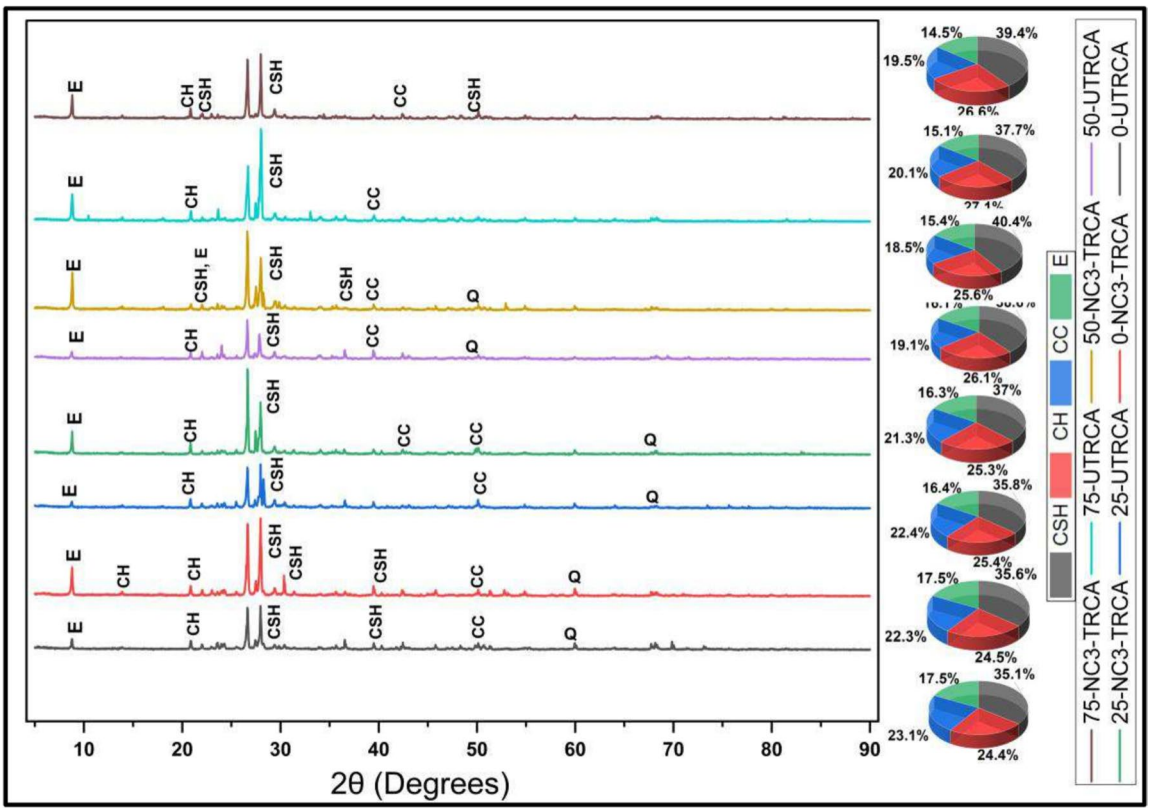

Fig. 7 XRD characterization of NS-treated TRCA and UTRCA

ratios represent decremental as the increase of adhered mortar content. Figure 9 represents the relation between crushing strength of aggregate vs elements identified.

In confidence to previous studies of Tantri et al. and A.U et al. [29, 34, 68], it is evident that the inverse relation with crushing strength of aggregate is observed for Ca/Si ratios and direct relation is observed for Si/Al ratio. It thus confirms the element contribution for proper hydration process which results in stronger adhere mortar accompanied by the formation of additional CSH, CH, and CC. Overall, EDS, XRD, and FE-SEM findings are in line with physical characteristics of aggregates. Also, 50-NS-TRCA followed by 75-NS-TRCA are found to be optimally performing aggregates and shall be utilized for further investigations.

Table 4 Identification for the compound name and chemical formula of pastes

Identity	Ref. code	Compound name	Chemical formula
CSH	96–100-0047	Clinotobermorite	$Ca_5Si_6O_{18}H$
CH	96–100-8782	Portlandite	$Ca_1O_2H_2$
E	96–901-2923	Ettringite	$Ca_{12}A_{l4}S_6O_{100}H_{128}$
CC or $CaCO_3$	96–900-9668	Calcite	$Ca_6C_6O_{18}$

3 Mix design

3.1 Mix quantification

According to the TRCA's characterization, the identified high-performing aggregates are 50-NS-TRCA and 75-NS-TRCA, both of which have been used entirely in the concrete. Ternary proportions, with mixes of OPC, FFA, and WCP, will take on additional binder phase responsibility in the intended concrete. To further understand the impact of WCP on NS-treated TRCA, FFA was gradually replaced with WCP at a 10% incremental rate in the concrete mix, which eventually increased from 0 to 50%. All concrete mixes which include natural aggregate (NA), TRCA-, and UTRCA-based concrete proportions are prepared based on IS 10262–2019 [69] and are presented in Table 6. In the present study, CM of M40 is the stand-alone mix performed with 100% OPC and by incorporating 100% natural coarse aggregates (NCA), and only two specific overall ideal mixes are used to showcase the performance of UTRCA. All prepared concrete mixes maintain a water binder ratio of about 0.3% to understand the performance of other variables on the same. All concrete mixes had a high range water reducer based on polycarboxylate ether, which reduced the need for water content and produced the desired workability.

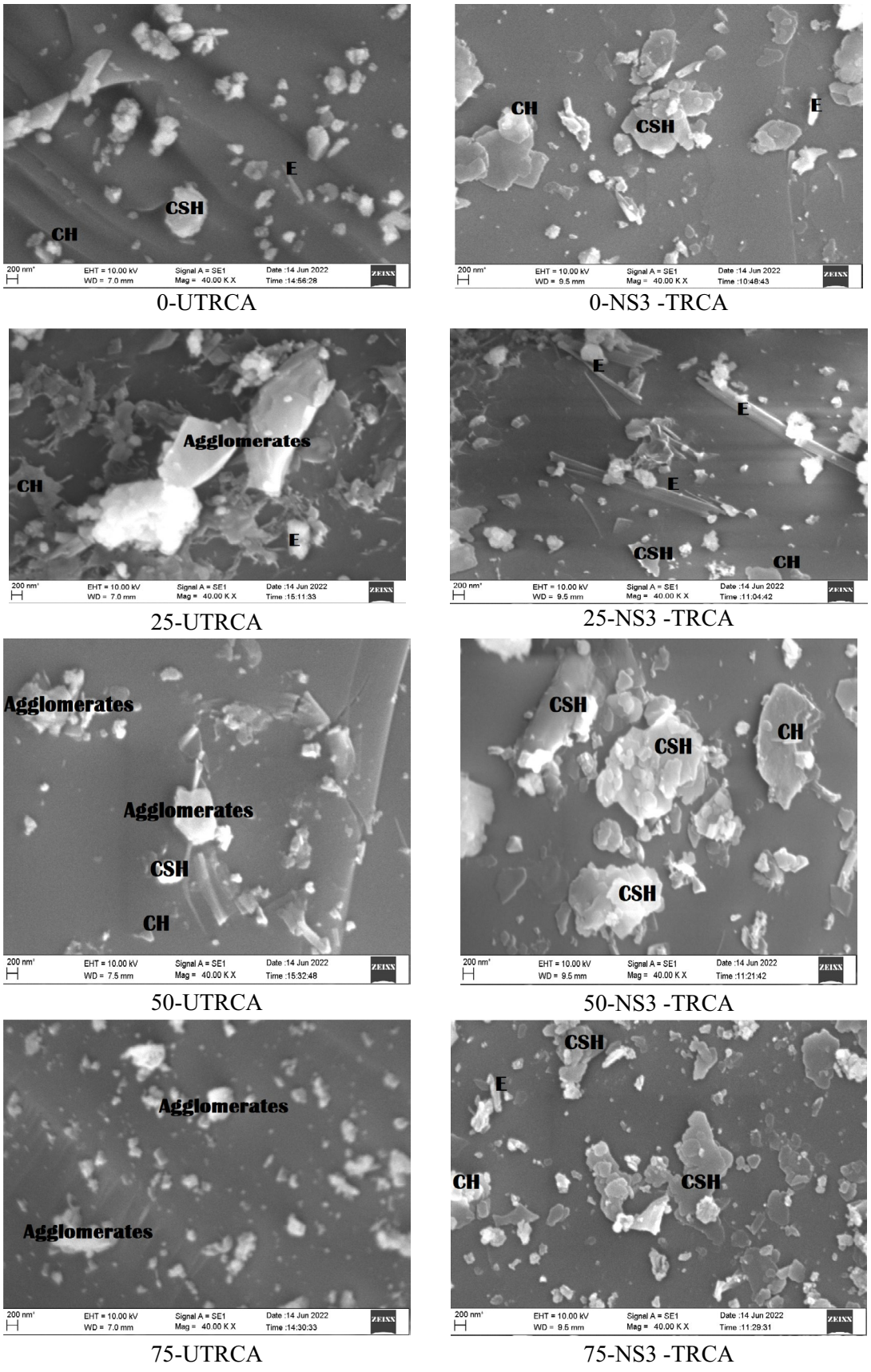

Fig. 8 FE-SEM (scale 200 nm) characterization of NS-treated TRCA and UTRCA

Table 5 EDS characterization of NS-treated TRCA

Aggregates	Si	Al	Ca	Si + Al	Si/Al	Ca/(Si + Al)	Ca/Si	Ca/Al
0-NS3-TRCA	14	0.45	9.39	14.45	31.11	0.65	0.68	20.87
25-NS3-TRCA	14.67	0.51	10.33	15.18	28.76	0.68	0.71	20.25
50-NS3-TRCA	20	0.83	15.66	20.83	24.09	0.75	0.78	18.87
75-NS3-TRCA	18.17	0.67	13.02	18.84	27.12	0.69	0.72	19.43

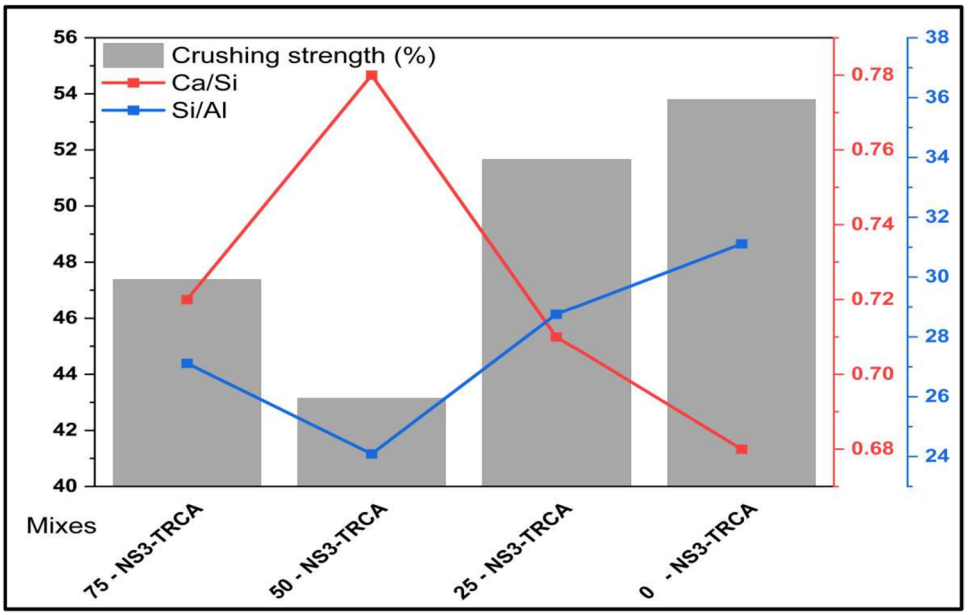

Fig. 9 Elements ratio vs crushing strength characterization of NS-treated TRCA

3.2 Test design

Test designs on concrete were performed in four stages which were (i) physical characterization, (ii) quality characterization, (iii) durability characterization, and (iv) microstructure characterization on concrete binders. Detail chart of test design is presented in Table 7.

i. Physical characterization involves predesigned mechanical tests as per IS codes which were conducted through compressive strength on concrete cube, flexural strength on concrete beam, split tensile strength, and modulus of elasticity on concrete cylinder. All the tests were performed at ambient room temperature of about 27 °C ± 2 °C.
ii. Quality characterization through ultrasonic pulse velocity (UPV) was performed on concrete cube using T-I-C-O ULTRASONIC INSTRUMENT, supplied by PROCEQSA, Switzerland, at ambient room temperature of about 27 °C ± 2 °C for 28-day aged samples. Although density and water absorption tests were performed on concrete cube using BS 1881–122–198 [70] at the age of 28 days at room temperature about 27 °C ± 2 °C.
iii. Durability characterization studied by performing the acid and alkalinity resistance of ternary paste bounded NA/TRCA and UTRCA incorporated concrete. The acid test was performed on 150-mm sized concrete cubes utilising hydrochloric (HCL) acid concentration of about 5% by weight of water (pH = 1) on a plastic container for the duration of 28th, 90th, and 148th days (days accounted after 28 days of normal curing). If the pH of the solution dropped, more concentrated hydrochloric acid was added to restore the pH that was needed. After every 30-day interval, a new 1% of hydrochloric acid solution was replaced by the old solution. Weight loss and compression strength were measured for every 15 days up to 148 days. Meanwhile, alkalinity resistance performed with 150-mm sized concrete cubes utilising sea water (pH = 8.3 to 8.7) solution for the duration of 28th, 90th, and 148th days (days accounted after 28 days of normal curing). After every 30-day interval, a new sea water solution was replaced by the old solution.
iv. Microstructure characterization on concrete binders was analysed through field emission scanning electron microscopy (FE-SEM) to understand the morphology, energy dispersive spectroscopy (EDS) to understand

Table 6 Mix proportions of concrete mixes as per IS 10262–2019 [69]

Identities	OPC (kg/m^3)	FFA (kg/m^3)	WCP (kg/m^3)	Water (kg/m^3)	Aggregate details			
					PQD sand (kg/m^3)	NCA	NS3-TRCA	UTRCA
CM	450	-	-	180	648	996		
50-NS3-TRCA-WCP0	225	225	-	180	646		1041	
50-NS3-TRCA-WCP10	225	180	45	180	646		1041	
50-NS3-TRCA-WCP20	225	135	90	180	646		1041	
50-NS3-TRCA-WCP30*	225	90	135	180	646		1041	
50-NS3-TRCA-WCP40	225	45	180	180	646		1041	
50-NS3-TRCA-WCP50	225	-	225	180	646		1041	
75-NS3-TRCA-WCP0	225	225	-	180	646		1041	
75-NS3-TRCA-WCP10	225	180	45	180	646		1041	
75-NS3-TRCA-WCP20*	225	135	90	180	646		1041	
75-NS3-TRCA-WCP30	225	90	135	180	646		1041	
75-NS3-TRCA-WCP40	225	45	180	180	646		1041	
75-NS3-TRCA-WCP50	225	-	225	180	646		1041	
50-UTRCA-WCP30	225	90	135	180	646			1039
75-UTRCA-WCP20	225	90	135	180	646			1039

High range water reducer/superplasticizer has been added about 0.9% by the weight of cementitious material for all above mentioned concrete mixes

*Indicates optimized mix

Identity description example: "50-NS3-TRCA-WCP30" represents 50% of adhered mortar in recycled concrete aggregate (RCA); NS3 represents nano-silica (3%) treatment for adhered mortar of RCA; TRCA represents treated RCA; WCP30 represents 30% of waste ceramic powder incorporation as a cementitious material.

the element and their chemical relationships, X-ray diffraction analysis (XRD) to investigate the crystallographic structure followed by its chemical composition, and Fourier transform infra-red (FTIR) to identify and distinguish among chemical bonds.

4 Physical characteristics of concrete

4.1 Compressive strength

The key factor used to characterize concrete is its compressive strength. The increase in WCP content up to 30% for 50-NS3-TRCA-based concrete mixes and up to 20% for 75-NS3-TRCA-based concrete mixes reflects increased compressive strength as shown in Fig. 10. The increase in WCP in ternary binder and adhered mortar treated with nano-silica succeeded in representing dense ITS owing to increased pozzolanic reactivity, which is the major reason for increment of compressive strength [46, 71]. For the 50-NS3-TRCA and 75-NS3-TRCA, respectively, with further incremental WCP at 40% and at 30%, a declining trend in compressive strength is observed. It might be due to presence of excessive pozzolana material, which slows down the hydration reaction causing neutral phase in later stages of secondary reactions with other constituents [34]. Overall, 50-NS3-TRCA-WCP30* and 75-NS3-TRCA-WCP20* were determined to be ideal because they had compressive strengths that were 18.33% and 6.68% higher than CM. Additionally, an optimal mix with UTRCA was performed to comprehend the influence of TRCA over UTRCA. It was discovered that 50-NS3-TRCA-WCP30* and 75-NS3-TRCA-WCP20* have greater compressive strengths than 50-UTRCA-WCP30* and 75-URCA-WCP20*, respectively, by 48.10% and 8.52%. The finer texture of WCP (average particle diameter 6.01 (μm) than FFA and OPC (refer Fig. 2)) is attributed to the progressive reaction which results in additional CSH, CH, and CC gels. Additionally, the presence of nano-silica in TRCA increases CSH formations when it reacts with the ternary binders. Microstructural studies with FE-SEM, EDX, XRD, FTIR, and TGA are reviewed in detail and are found to be consistent with findings on compression strength.

4.2 Split tensile strength

Concrete's secondary quality is split tensile strength, which is shown in Fig. 11 precisely exhibiting the same trend as the compression strength. The best-performing concrete as seen

Table 7 Test design chart

Sample details	Test executed	Sample geometry	Instrument	Standards	Age schedule
Physical characterization of concrete	Compressive strength (CS)	Cube 150*150*150 mm	CTM 3000KN	IS 516–1959	7th, 28th, 90th
	Split tensile strength (STS)	Cylinder-Día 150 mm and verticle-300 mm	CTM 3000KN	IS 5816–1999	7th, 28th, 90th
	Flexural strength (FS)	Prism-100 × 100 × 500 mm	UTM	IS 516–1959	7th, 28th, 90th
	Modulus of elasticity (MoE)	Cylinder-Día 150 mm and verticle-300 mm	UTM and LVDT arrangements	IS 516–1959	28th
Quality characterization of concrete	Ultrasonic pulse velocity (UPV)	Cube 150*150*150 mm	PUNDIT inst	IS 13311–1–1992	28th
	Water absorption	Cube 150*150*150 mm	-	BS 1881–122–198	28th
	Density	Cube 150*150*150 mm	-	BS 1881–122–198	28th
Durability characterization on concrete	Concrete expose to acid attack (AA)–hydrochloric (HCL) acid	Cube 150*150*150 mm	CS test on CTM 3000KN	-	Days after 28 days of normal curing—28th, 90th, 148th
	Concrete expose to sea water	Cube 150*150*150 mm	CS test on CTM 3000KN	-	Days after 28 days of normal curing—28th, 90th, 148th
Microstructure characterization on binders	FESEM	10 × 10 × 10 mm	Carl Zeiss, Oxford instrument	-	Days at 28th of normal curing and 148th after exposure
	EDS	10 × 10 × 10 mm	Carl Zeiss, Oxford instrument	-	Days at 28th of normal curing and 148th after exposure
	XRD	Powder (< 45 μ)	Rigaku Mini-flex JASCO	-	Days at 28th of normal curing and 148th after exposure
	FTIR	Powder (< 45 μ)	JASCO FTIR 6300	-	Days at 28th of normal curing and 148th after exposure

from Fig. 11 is 50-NS3-TRCA-WCP30* and 75-NS3-TRCA-WCP20*. The reason being increased aggregate interlocking and mortar bond properties. The lowest split tensile strengths for mixes 50-NS-TRCA-WCP0 and 75-NS3-TRCA-WCP0 are around 9.072% and 10.679% lower than CM at the age of 7 days, respectively. However, mixes (50-NS3-TRCA-WCP0 and 75-NS3-TRCA-WCP0) are successful in representing the same split tensile strength as CM at the higher curing ages. When 50-NS3-TRCA-WCP30* and 75-NS3-TRCA-WCP20* were compared to 50-UTRCA-WCP30 and 75-UTRCA-WCP20, it was found that TRCA performed better because it had higher split tensile strengths at various ages: 18.012% and 13.98% at 7 days, 13.583% and 6.78% at 28 days, and 9.58% and 5.68% at 90 days, respectively. The use of WCP and nano-silica soaked, steam cured RCA improved the split tensile strength of concrete by consuming more of the hydrated calcium silicate phase Ca $(OH)_2$ in the binder composite, which is consistent with earlier findings [12, 16, 72, 73]. With higher R^2 values of about 0.96, Fig. 12 depicts a linear relationship between the square root of concrete's compressive strength and its split tensile strength demonstrating how they are significantly related to one another.

4.3 Flexural strength of concrete

The flexural properties of concrete are ascertained using a two-point loading approach, results showcased as in Fig. 13. When compared to UTRCA, WCP incorporation in TRCA represents incremental results. In comparison to 50-UTRCA-WCP30 and 75-UTRCA-WCP20, 50-NS3-TRCA-WCP30* and 75-NS3-TRCA-WCP20* indicate incremental flexural strength of around 14.08% and 10.77% at 7-day curing period, 14.68% and 7.80% at 28-day curing period, and 8% and 4.70% at 90-day curing period. Additionally, a comparison of 50-NS3-TRCA and 75-NS3-TRCA showcased that 50-NS3-TRCA performed at its best. The combined effects of increased pozzolanic activity of nano-silica and enhanced

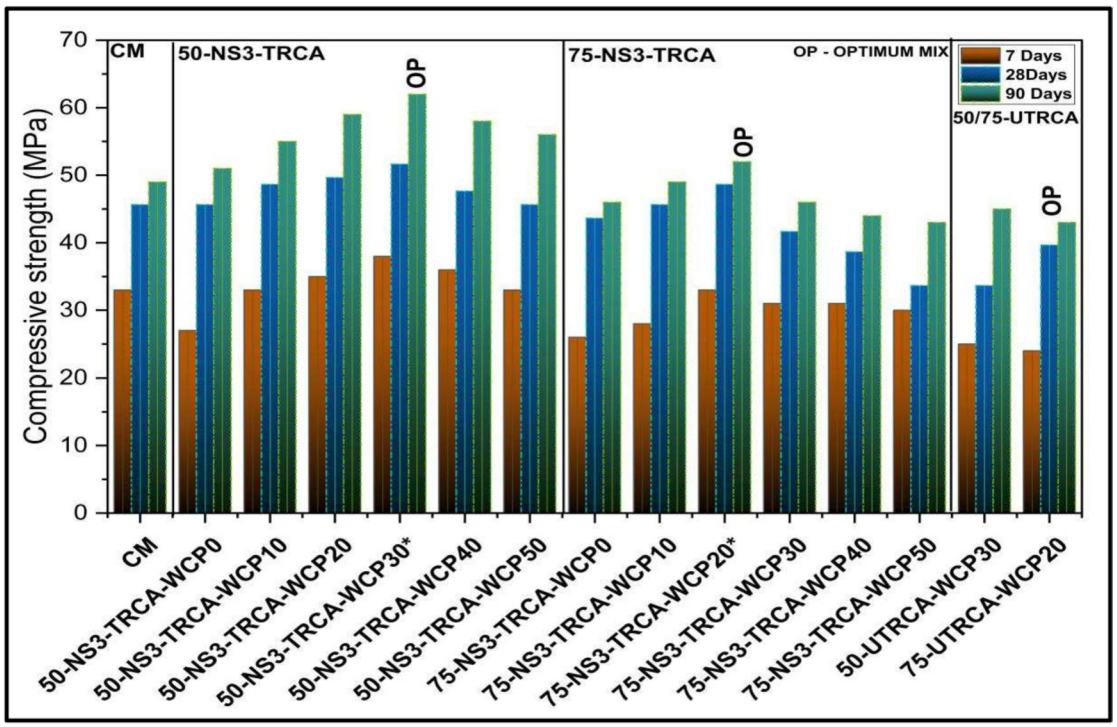

Fig. 10 Compressive strength of concrete mixes

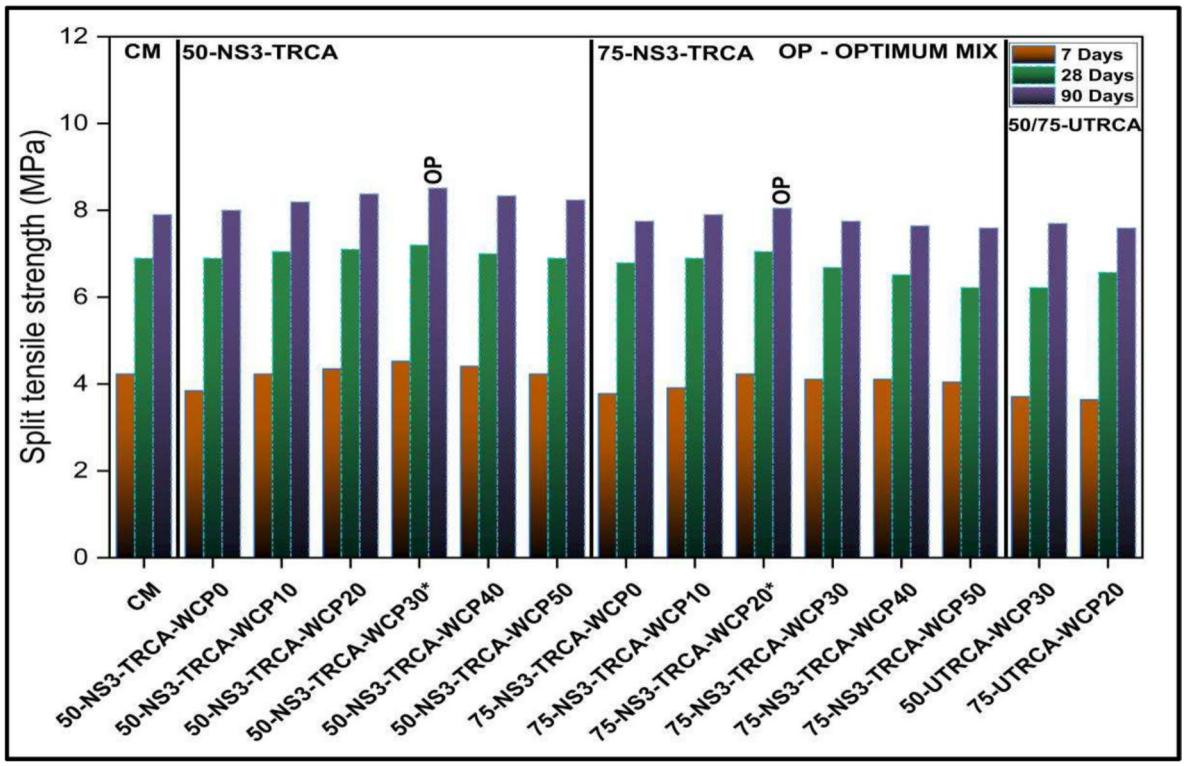

Fig. 11 Split tensile strength of concrete mixes

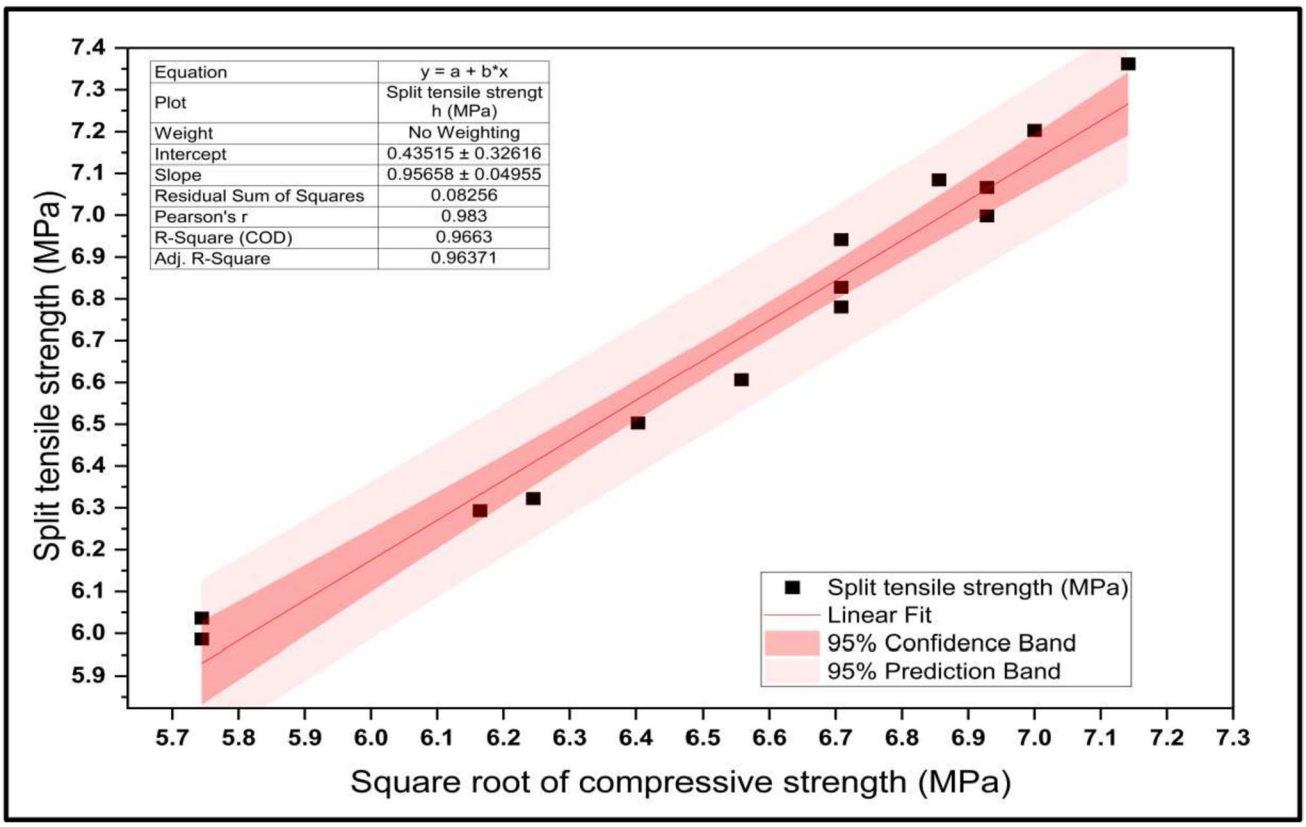

Fig. 12 $\sqrt{}$Compressive strength vs split tensile strength

bonding of ITZ of TRCA aggregate lead to higher improvements in flexural strength [32, 33, 74, 75]. Concrete's overall flexural strength follows a similar trend to that of its compressive strength and split tensile strength, both of which were thoroughly covered in the parts before this one (Sections 4.1 and 4.2). By showing a 0.96 R^2 value, Fig. 14 demonstrates the significant linear relationship between the concrete's flexural strength and compressive strength.

4.4 Modulus of elasticity

Through the elasticity's modulus, the relationship between stress and strain was examined after a 28-day curing period. The behaviour of the elastic modulus in relation to each concrete mix is shown in Fig. 15. The least results, was seen for 50-UTRCA-WCP30 of, 30.46 GPa. In contrast, 50-NS3-TRCA-WCP30* exhibited overall peak performance by having a 33.75% (43.74 GPa) higher modulus of elasticity than 50-UTRCA-WCP30 mix. It is abundantly clear that 3% nano-silica treatment to RCA improves the elasticity property in concrete by reducing the pores in adhered mortar and replacing them with CSH, CH, and then ettringites crystals (refer to Figs. 7, 8, and 9), as confirmed by microstructure characterization of TRCA through XRD, FE-SEM, and EDS (refer to Section 2.4). Regarding the adaptation of the 75% adhere mortar treatment technique, the 75-NS3-TRCA-WCP20* represents the best performance by achieving a greater modulus of elasticity than the 75-UTRCA-WCP20 by around 13.80% (37.62 GPa). Additionally, as shown in Fig. 16, the relation between compressive strength and modulus of elasticity (GPa) is significant, with an R^2 value of 0.80. Overall findings of concrete's modulus of elastic behaviour are consistent with the material's compression, split tensile strength, and flexural properties.

5 Quality characteristics of concrete

Ultrasonic pulse velocity (UPV) test conducted to determine the quality of concrete regards to aggregate packing, density, and water absorption characteristics of concrete. From 3100 m/s for the 50-UTRCA-WCP30 to 5101 m/s for the 50-NS3-TRCA-WCP30*, there is an overall change in UPV values. An improvement of 64.54% in UPV clearly shows how NS3 treatment followed by steam treatment, a revolutionary method, increased the bonding properties of adhering mortar. In addition to this, comparison of 75-UTRCA-WCP20 with 75-NS3-TRCA-WCP20* represents 23.94%

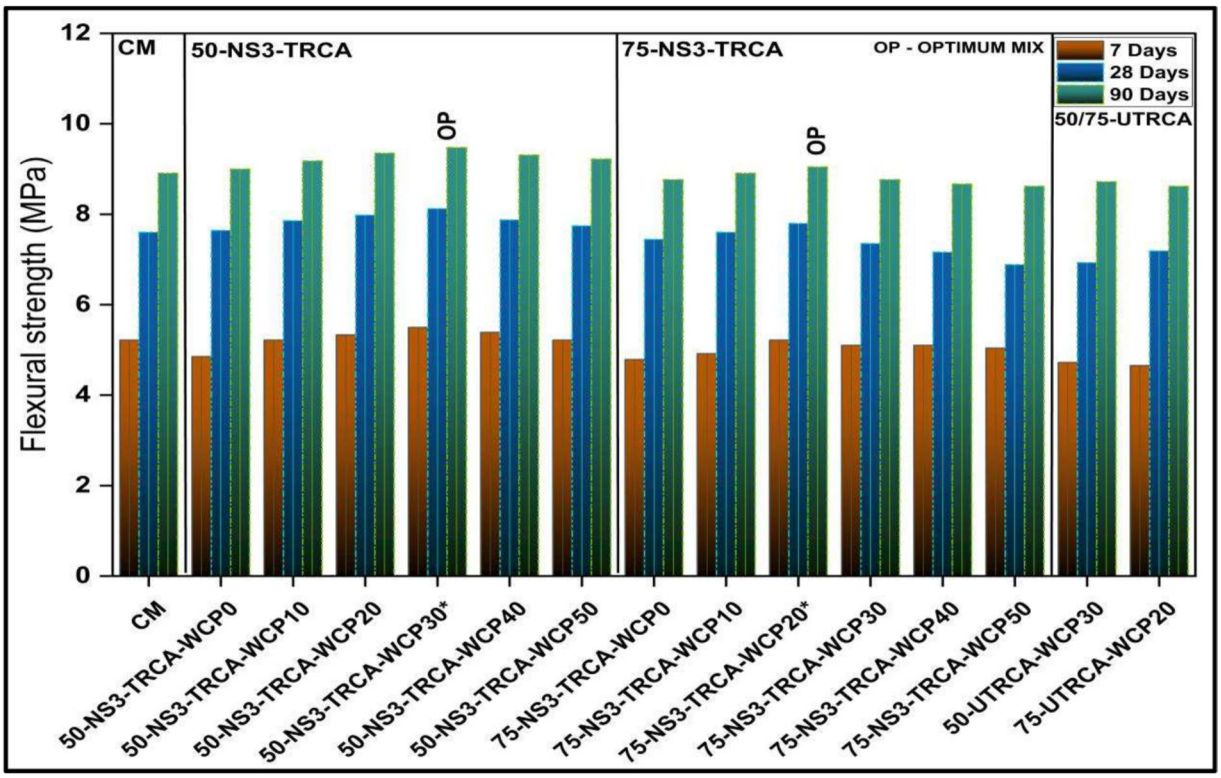

Fig. 13 Flexural strength of concrete mixes

increased UPV performance for 75-NS5-TRCA-WCP20*. Furthermore, comparison of CM with 50-NS3-TRCA-WCP30* and 75-NS3-TRCA-WCP20* demonstrated increase of 15.69% and 3.33% in UPV performance for TRCA respectively. Reason being that by reducing the pore structure with reference to adhering mortar followed by WCP-based ternary binder system, the influence of nano-silica and WCP-based ternary binder system has a higher impact on the creation of dense microstructure, improving ITZ interlocking with TRCA. Furthermore, it is confirmed regards to previous microstructural characterization of TRCA aggregates as presented in Fig. 7, Fig. 8, and Fig. 9, which represents increase of CSH gels leading to strong adhered mortar physical characteristics. Meanwhile, compressive strength and density of concrete represent same trend as that of UPV performances as shown in Fig. 17. Density of concrete varied from 2295 kg/m^3 (for 50-UTRCA-WCP30) to 2451 kg/m^3 (for 50-NS3-TRCA-WCP30*), which represents increase of 6.79% in density. Followed by 75-NS3-TRCA-WCP20* representing 5.79% incremental density (2428 kg/m^3) as compared to 75-UTRCA-WCP20 mix (2295 kg/m^3). Density comparison of CM with 50-NS3-TRCA-WCP30* and 75-NS3-TRCA-WCP20* revealed increments of 2.30% and 1.33% in density respectively. Water absorption characteristics of concrete are inversely proportional to UPV, compressive strength, and density characteristics of concrete. The percentage of water absorption in concrete ranged from 2.66% for concrete mix 50-UTRCA-WCP30 to 1.74% for concrete mix 50-NS3-TRCA-WCP30*, wherein the 50-NS3-TRCA-WCP30* blend showed a reduction in water absorption by 0.92%. When compared to 75-UTRCA-WCP20, 75-NS3-TRCA-WCP20* showed a 0.8% reduction in water absorption. Furthermore, when CM was compared to mixes of 50-NS3-TRCA-WCP30* and 75-NS3-TRCA-WCP20*, the amounts of water absorption decreased by 0.56% and 0.44%, respectively. Figure 18 represents R^2 value of around 0.98, 0.98, and 0.88, highlighting the considerable association between concrete's compressive strength and UPV, density, and water absorption properties respectively. It is observed that the mechanical properties of concrete match the qualities of concrete as a whole.

6 Durability characterization on concrete

6.1 Concrete expose to acid attack (AA)–hydrochloric (HCL) acid

Reduction in compressive strength and weight loss found for concrete mixes while exposed to concentrated HCL solution (pH = 1) for a duration of 28 days, 90 days, and 148 days

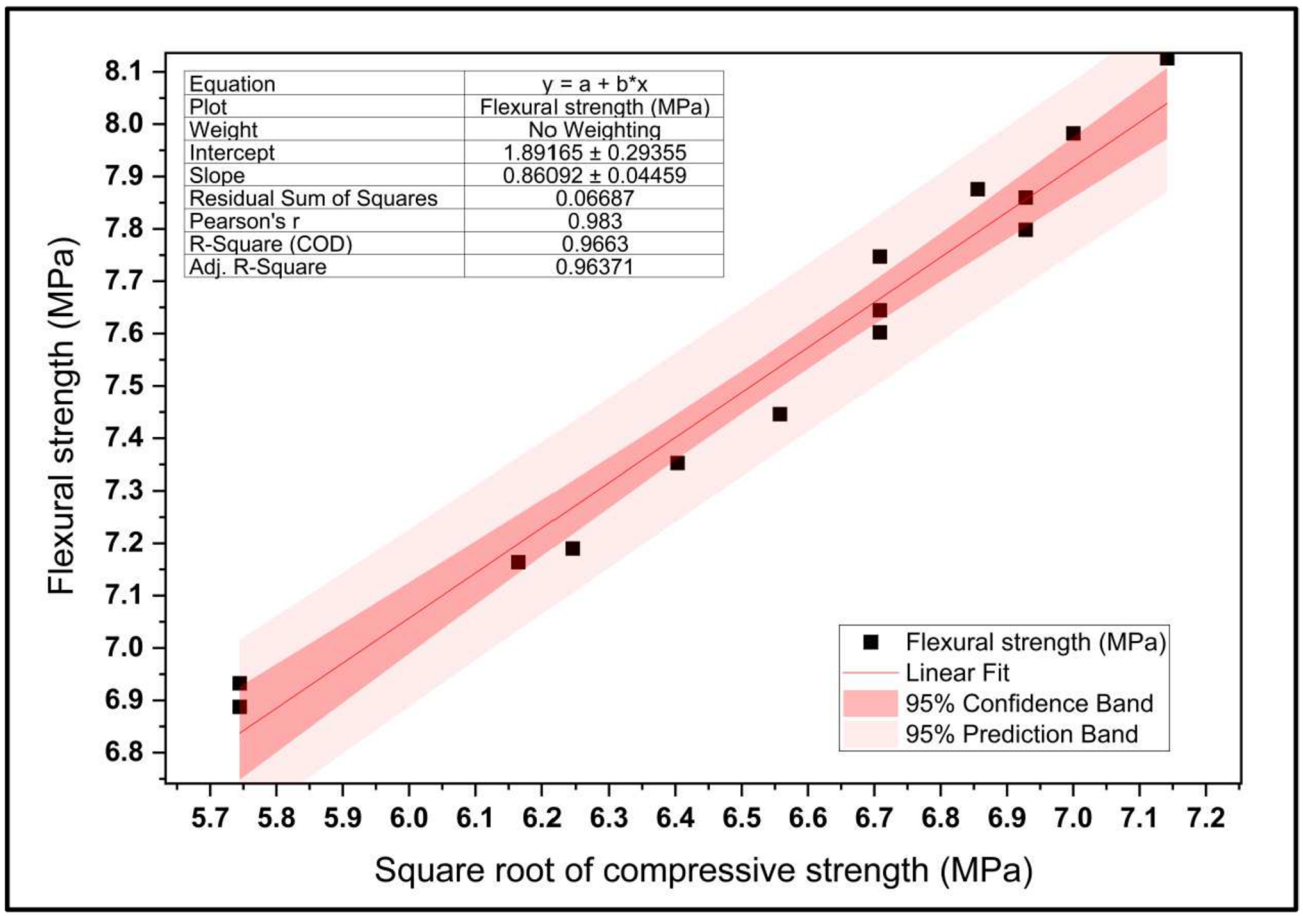

Fig. 14 $\sqrt{\text{Compressive strength}}$ vs flexural strength

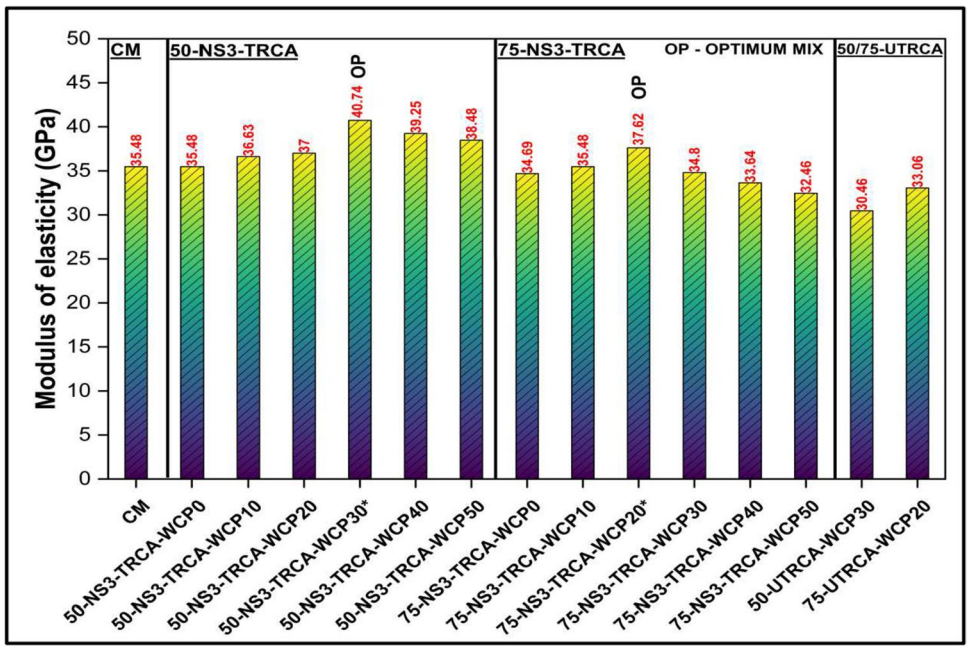

Fig. 15 Modulus of elasticity of concrete mixes at 28-day curing period

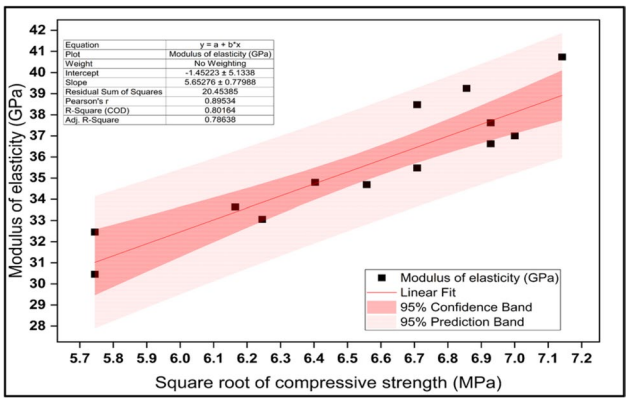

Fig. 16 $\sqrt{\text{Compressive strength}}$ vs modulus of elasticity (GPa)

is shown in Fig. 19. It is seen from Fig. 19 that there is a progressive reduction of compressive strength and percentage weight loss with regard to days of exposure. Overall, 50-NS3-TRCA-WCP30* mix performs better having succeeded in resisting acid attack by representing low reduction in compressive strength and weight loss of about 4.75% and 39.75% at 28th day, 40.23% and 2.36% at 90th day, and 18.96% and 24.52% at 148th days respectively. With regard to 75-TRCA, better resistance to acid attack was represented by 75-NS3-TRCA-WCP20*, which was found to have low reduction in compressive strength and weight loss of about 13.22%, 48.22% and 48.82% and 11.85%, 27.9% and 32.54% at 28th, 90th, and 148th days respectively. Under the influence of this acid environment, the hydrated products of ternary binder portlandite dissolve and cause the CSH structure to decalcify, leaving an extremely porous corroded layer in binders that lowers compressive strength [76, 77]. When a particular acid combines with calcium molecules, it produces calcium chloride which is very soluble [48, 78] and hence the weight loss. However, the nano-silica prioritized steam treatment verifies the formation of more CSH gels rather than portlandite ($Ca(OH)_2$), which is the explanation for the higher performance of 50-NS3-TRCA-WCP30* and 75-NS3-TRCA-WCP20* mixes (refer to Fig. 7). Additionally, as evidenced by microstructural evaluation (refer to Section 7), waste ceramic powder-based ternary systems promote the formation of additional CSH gels. Low lime content in ternary binders' mixes is also an advantage, as it results in slower degradation and greater resistance when compared to OPC-based CM when exposed to acid environments. Additionally, 50-UTRCA-WCP30 exhibits better performance in terms of UTRCA than 75-UTRCA-WCP20, which revealed that the presence of too much older adhered mortar causes faster deterioration in the form of CSH decalcification and gypsum production, which leads to volume instability caused due to formation of gypsum leading to

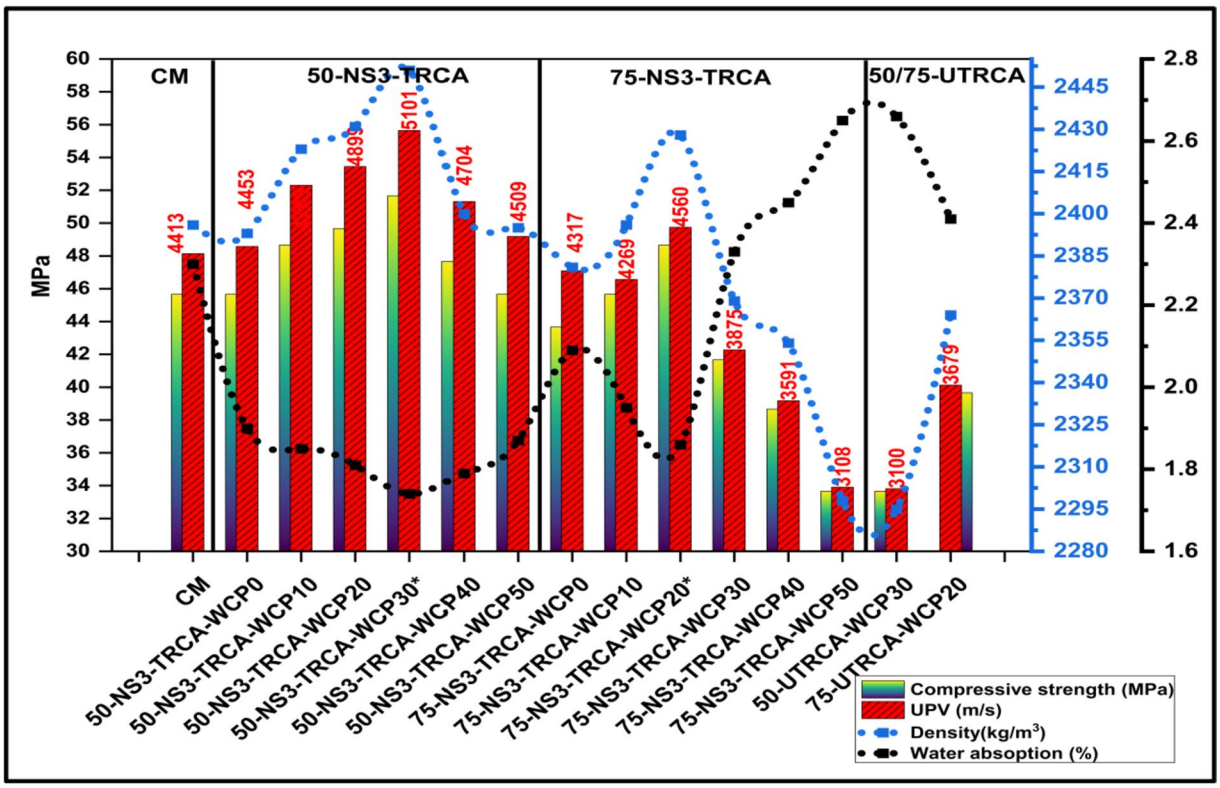

Fig. 17 Quality characterization of concrete mixes

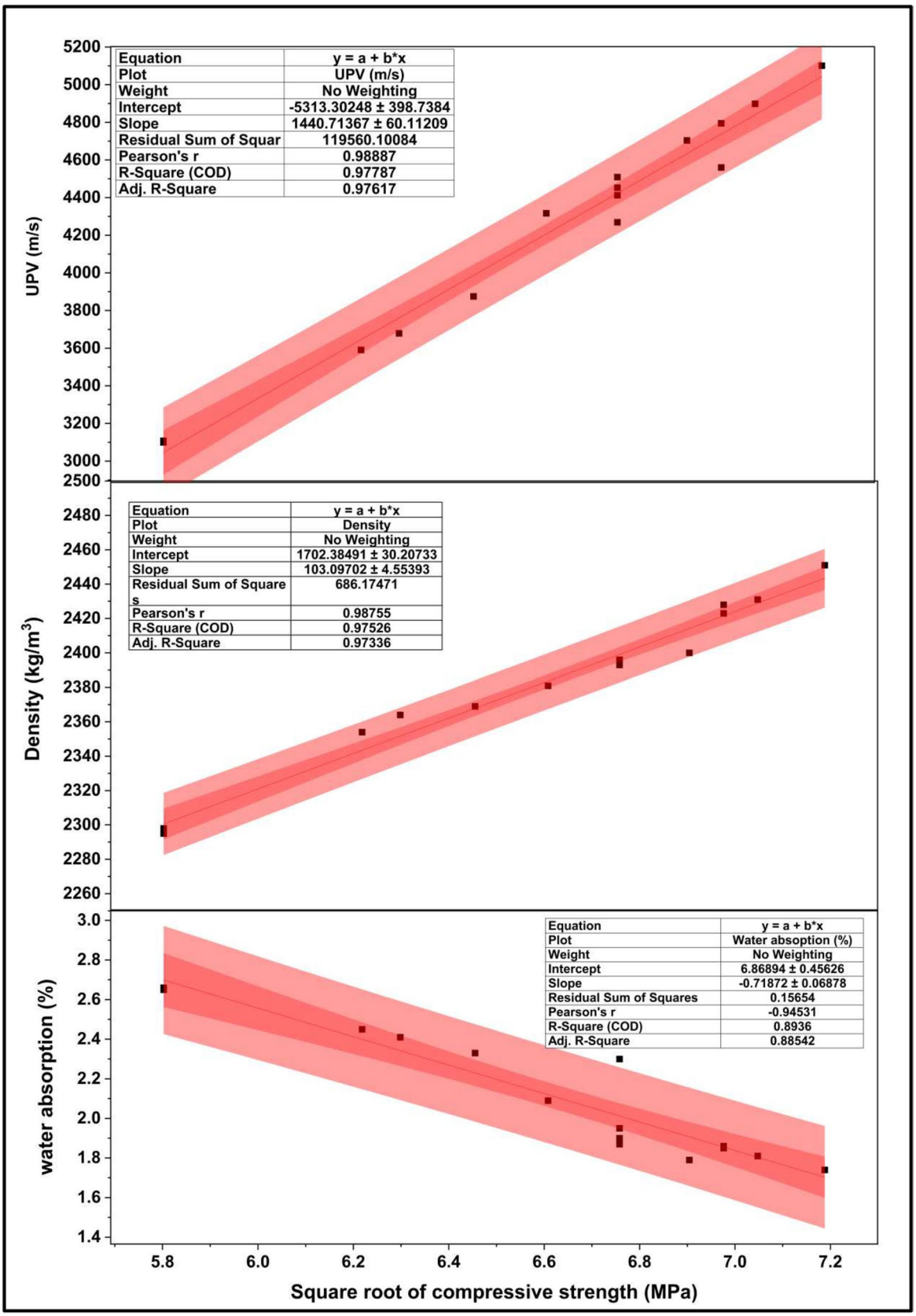

Fig. 18 $\sqrt{\text{Compressive strength}}$ vs quality characterization of concrete mixes

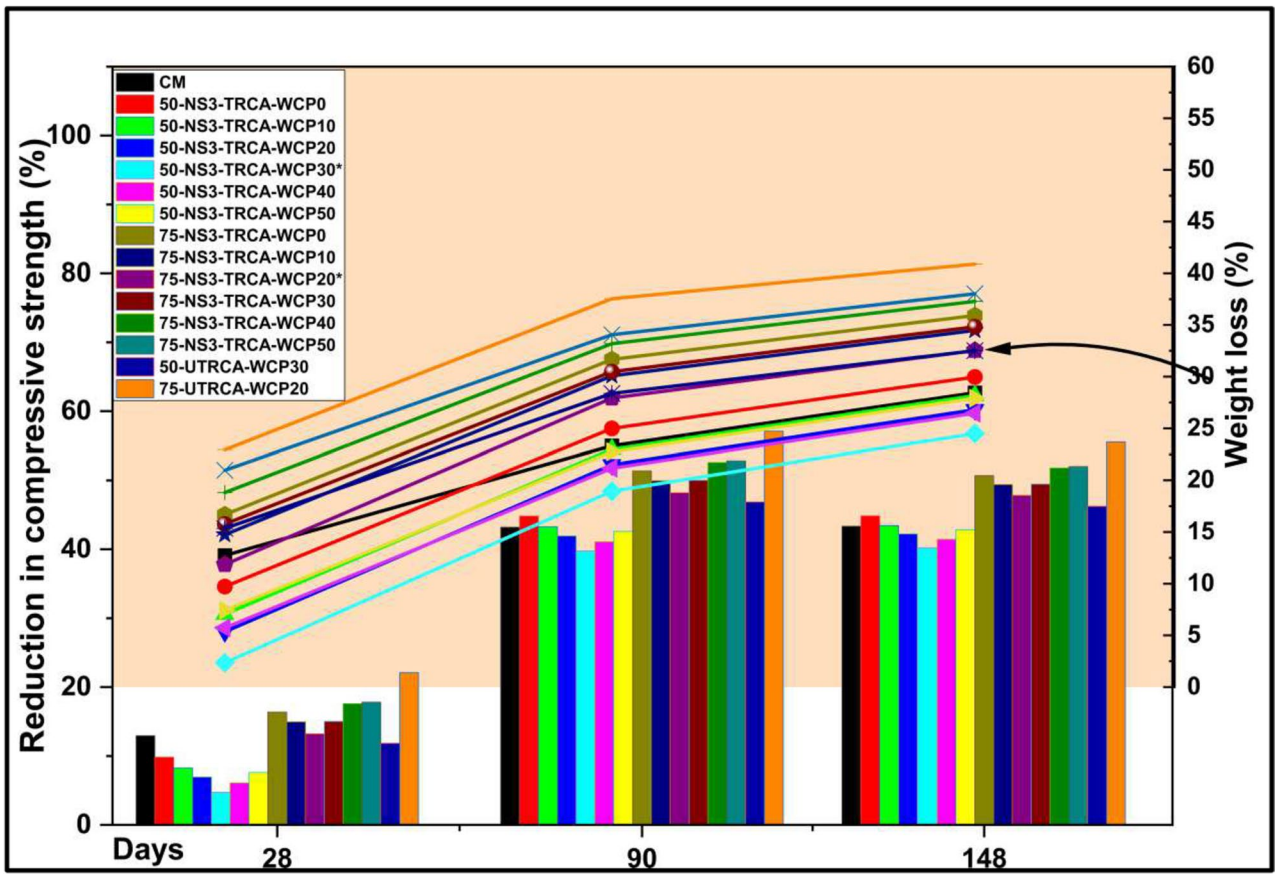

Fig. 19 % reduction in compressive strength and weight loss of concrete while expose to HCL acid

decrease in % of weight and compressive strength [79]. By the age of 148 days, calcium from the aggregates has been leached away, resulting in decaying, smoother aggregate structure. This expanding strain on the binder pastes causes cracking and failure of the concrete. Overall, 50-NS3-TRCA-WCP30* concrete mix is found to better resist the acid attack.

6.2 Concrete expose to sea water

For the period of the 28th, 90th, and 148th ages, the resistance of concrete to sea water exposure is assessed in terms of a decline in compressive strength and a percentage of weight loss, as shown in Fig. 20. Results show that the 50-NS3-TRCA-WCP30* blend exhibits substantially greater resistance to saltwater, as seen by improvements with regard to least reduction in compressive strength of 1.26%, 5.00%, and 12.07%, followed by losses in weight of 1.53%, 3.32%, and 5.93% for 28th, 90th, and 148th days respectively. Among 75-TRCA mixes, 75-NS3-TRCA-WCP20* mix showed lower reduction in compressive strength and weight loss of approximately 5.63%, 14.40%, 21.184% and 7.70%, 9.14%, 11.15% at 28th, 90th, and 148th days, respectively. The interaction between magnesium sulphate from seawater and calcium hydroxide from a ternary binder system result in calcium sulphate and magnesium hydroxide precipitation [80, 81]. Calcium sulpho-aluminate is created by combining magnesium sulphate with hydrated calcium aluminate. These latter kinds are the main causes of concrete's compressive strength loss and weight loss features [55, 58, 60]. The lime component of the concrete was also lost due to leaching. Calcium hydroxide and calcium sulphate are easily soluble in saltwater, and hence leaching activity will be accelerated [50, 82]. Additionally, the abrasive properties of salts found in sea water cause the adhering mortar of concrete to deteriorate, which is a secondary cause of concrete degradation [80, 81]. However, there was a noticeably smaller percentage effect on the 50-NS3-TRCA-WCP30* and 75-NS3-TRCA-WCP20* mixes because of the increased microstructural, chemical, and physical (see Section 2.4) properties of TRCA aggregates prior to mixing with ternary blends that included WCP. Further comparison of UTRCA-based concrete mixes showed that 50-UTRCA-WCP30 exhibits better performance in terms of UTRCA than 75-UTRCA-WCP20, representing higher resistance to reduction in compressive strength characteristics by 6.01%, 5.80%, and 5.19%, followed by

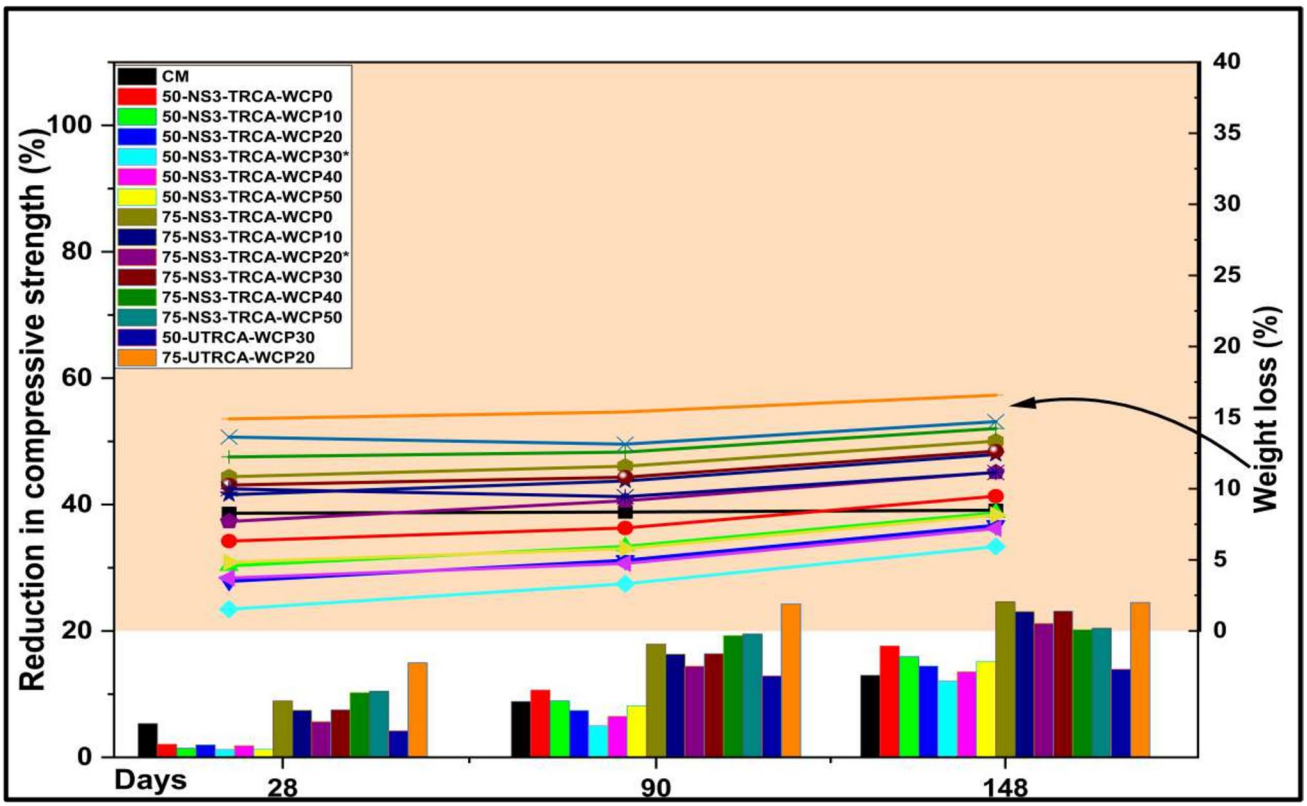

Fig. 20 % reduction in compressive strength and weight loss of concrete while expose to sea water

lower weight loss percentages by 4.92%, 5.95%, and 5.43% with regard to 28th, 90th, and 148th ages respectively. The reason for this is the presence of more untreated adhered mortar which will accelerate the process of replacing the Mg^{2+} ion with Ca^{2+} in the CSH to produce magnesium silicate hydrate, which is purportedly non-cementitious [77]. This causes the Ca/Si ratio in the CSH of the adhered mortar to drop, which causes failure by producing more pores and cracks.

7 Microstructure characterization on binders

7.1 FE-SEM

As shown in Fig. 21, the ternary paste bonded adhered mortar of 50-NS3-TRCA-WCP30* was meticulously examined using FE-SEM image analysis at 1-μm scale with 10 to 20 KX magnification and taking 6.5- to 7.5-mm widen area into consideration for 28 days of water cured sample, 148 days of HCL exposure sample, and 148 days of sea water exposure sample. The 50-NS3-TRCA-WCP30* 28-day water-cured mortar sample showed a dense, void-free structure and 99% hydration by accumulating the most calcium silicate hydrates, followed by calcium carbonate, calcium hydroxide, and ettringites. It was the obvious cause of the 50-NS3-TRCA-WCP30* concrete's optimal mechanical performance, which included its compressive, tensile, flexural, and elastic modulus qualities as previously discussed in Section 4. In addition, the void free crystalline dense structure of 50-NS3-TRCA-WCP30* mortar in concrete mix consolidates the evidence for more impervious nature, least water absorption characteristics followed by optimum UPV performance compared to all other concrete mixes as discussed in detail and presented through results in Section 5. Additionally, when 50-NS3-TRCA-WCP30* mix was exposed to HCL solution, FE-SEM imaging showed that the CSH structure was decalcified, which caused the mortar in the concrete to become more porous and display brittle behaviour. In particular, CSH lost solid stability and released majority of silica-coated lime, which is distinguished by white flushes as shown in the FE-SEM image that is being given in Fig. 21 [77, 83]. Furthermore, the formation of excess gypsum has been observed which is due to presence of silica in treated adhered mortar which demands excess space leading to micropressure and expansion of hydrated structure causing failure of mortar by leaching [48, 83, 84]. These findings are in line with compressive strength performance of HCL-exposed concrete samples

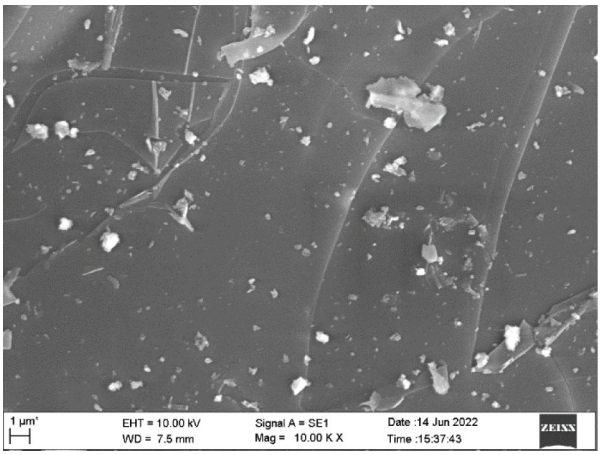

50-NS3-TRCA-WCP30* - 28 days water cured sample

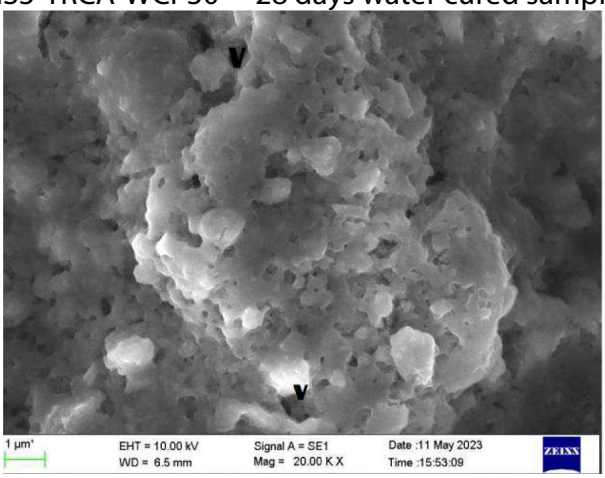

50-NS3-TRCA-WCP30* - 148 days HCL exposure sample

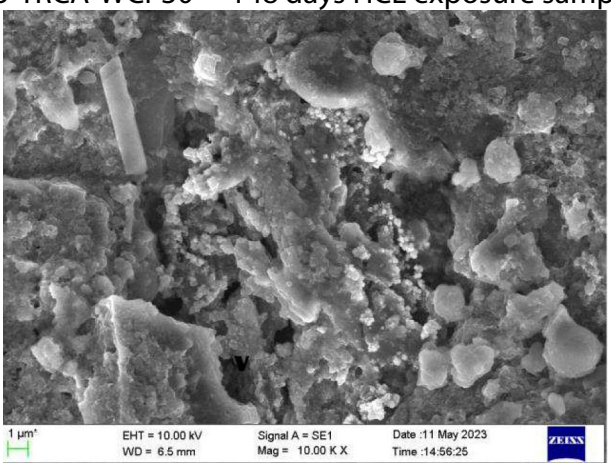

50-NS3-TRCA-WCP30* - 148 days Sea water exposure sample

Fig. 21 SEM image of optimum performed mix of 50-NS3-TRCA-WCP30*

as discussed in previous Section 6.1. Further FE-SEM images of mortar 50-NS3-TRCA-WCP30* exposed to sea water show porous oriented rough microtexture followed by salt deposits and decalcification of CSH, broken needle-like structure of ettringites due to harsh contact with salted sea water, and formation of gypsum due to pre-non-reacted additional silica present in pre-treated mortar are identified [59, 80, 81]. Compared to samples exposed to sea water, those exposed to HCL showed more robust decalcification of CSH. It is confirmed as described in Section 6.2 and is consistent with the sample compressive strength results after being exposed to sea water.

7.2 EDS

Table 8 shows the EDS analysis and correlation of the components found in the mortar made of 50-NS3-TRCA-WCP30* that is based on ternary binding pastes. According to the EDS data analysis, there is a conspicuous and current amalgamation of CSH gel. As the pre-nano-silica-treated adhered mortar reacts with the ternary binder, more CSH gel develops in the ternary system and Si element expands [74, 85]. As lower Ca/Si ratios are associated with the failure of microconcrete mortar, which is in line with the findings of FE-SEM, XRD, and FTIR analysis, it is confirmed and agrees with the mechanical performances of concrete mixes when exposed to HCL and sea water solutions. Though Ca/(Si + Al) and Si + Al reflect decreasing trend ratios, this may be the cause of the declining compressive strength performance of 50-NS3-TRCA-WCP30* concrete, as mentioned in Section 6.

7.3 XRD

The molecular components of the 50-NS3-TRCA-WCP30* mortar composed of WCP prioritized ternary paste binder + nano-silica-treated adhered mortar are carefully analysed using XRD analysis, as shown in Fig. 22. Table 9 lists the recognized Ref code, compound name, and chemical formula for the adhering mortar after it was subjected to portable water for 28 days, a HCL solution for 148 days, and a sea water solution for 148 days. When ternary pastes are applied to mortar which has been pre-treated with nano-silica and allowed to cure in water for 28 days, a distinctive semi-crystalline peak forms and new hydrated crystals are created. Identities reveal that the findings of $Ca_2SiO_4H_2O$ (CSH) (Ref-00–029-0373), $Ca(OH)_2$ in the form of portlandite (Ref-00–001-1079), $Ca_6Al_2O_6(OH)_6{\cdot}32H_2O$ (E) in form of ettringite (Ref-00–041-0216), $CaCO_3$ (CC) in the form of aragonite (Ref-00–005-0453), and SiO_2 (Q) in the form of

Table 8 EDS of ternary binding paste-based adhered mortar of 50-NS3-TRCA-WCP30*

Exposure conditions	Si	Al	Ca	Si + Al	Si/Al	Ca/(Si + Al)	Ca/Si
28-day water cured	18.39	5.44	18.91	23.83	3.38	0.79	1.03
148-day HCL exposure	10.35	3.11	9.32	13.46	3.33	0.69	0.90
148-day sea water	14.21	4.33	13.1	18.54	3.27	0.71	0.92

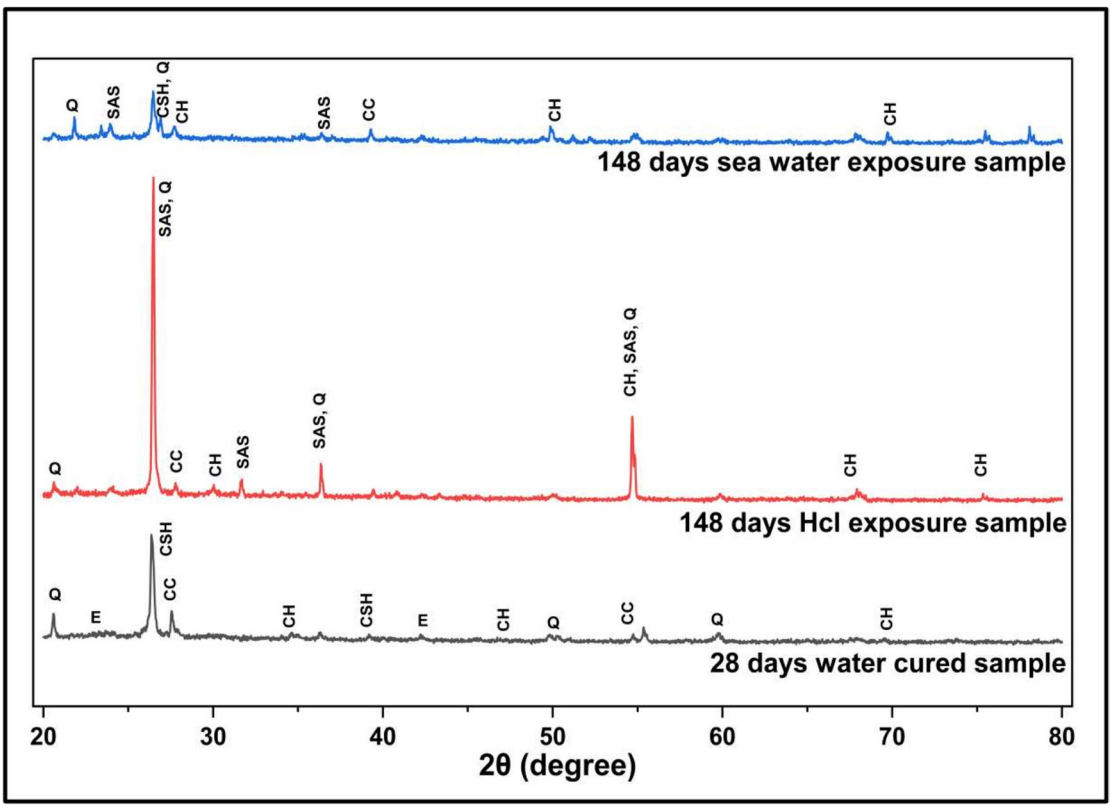

Fig. 22 XRD analysis of ternary binding paste-based adhered mortar of 50-NS3-TRCA-WCP30*

Table 9 Identification for the compound name and chemical formula of ternary binding paste-based adhered mortar of 50-NS3-TRCA-WCP30*

Identity	Ref. code	Compound name	Chemical formula
28-day water cured sample			
CSH	00–029-0373	Calcium silicate hydrate	$Ca_2SiO_4H_2O$
CH	00–001-1079	Portlandite	$Ca(OH)_2$
E	00–041-0216	Ettringite	$Ca_6Al_2O_6(OH)_6{\cdot}32H_2O$
CC	00–005-0453	Aragonite	$CaCO_3$
Q	00–046-1045	Quartz	SiO_2
148-day HCL exposure sample			
SAS	01–078-1995	Sodium aluminium silicate (albite)	Na ($AlSi_3O_8$)
CH	01–084-1274	Calcium hydroxide	Ca $(OH)_2$
CC	01–086-0174	Calcite, syn	$CaCO_3$
Q	01–083-0539	Quartz	SiO_2
148-day sea water exposure sample			
CSH	00–011-0595	Calcium silicate hydrate	$CaSi_2O_5{\cdot}2H_2O$
SAS	01–076-0898	Sodium aluminium silicate (albite)	Na ($AlSi_3O_8$)
CH	01–084-1267	Calcium hydroxide	$Ca(OH)_2$
CC	00–003-0893	Aragonite	$CaCO_3$
Q	01–083-2468	Quartz	SiO_2

quartz (Ref-00–046-1045) confirm the proper formation of dense and void free bonded structure as confirmed through FE-SEM and EDS analysis (refer to Sections 7.1 and 7.2). It confirms and in line with mechanical and quality characterization of concrete as previously discussed in Sections 4 and 5. Furthermore, with exposure to HCL solution for a duration of 148 days, decalcification of CSH has been confirmed by huge quantified identification of newly formed crystals called Na ($AlSi_3O_8$) in the form of albite (SAS) (Ref-01–078-1995), Ca $(OH)_2$ in the form of calcium hydroxide (CH) (Ref-01–084-1274), $CaCO_3$ (CC) in the form of calcite, and syn (Ref-01–086-0174) and SiO_2 in the form of quartz (Q) (Ref-01–083-0539). As it can be observed, after exposure to HCL solution, the intensity of CSH is least/absent and CH crystalline peaks are also reduced. These findings are in line with previous studies [49, 51, 77, 86, 87]. According to chemical reactions (Ca^{2+} $2(OH)^-$ $+SiO_2=C$ —S —H and Ca^{2+} $2(OH)^-$ $+Al_2$ $O_3=C$ —A —H), the product reaction between Ca $(OH)_2$ and HCL is $CaCl_2$ (calcium chloride) which is a soluble salt and can simply leach out of the mortar thereby deteriorating the mortar structure [87, 88]. Hence, this is the reason for reduction of compressive strength and weight parameters of concrete (refer to Section 6.1). But as compared to all other mixes, 50-NS3-TRCA-WCP30* performed better because the presence of WCP consumes more $Ca(OH)_2$ and produces C-S–H gel; thereby, the lowest intensity of $Ca(OH)_2$ is available for reaction with HCL [77, 87]. Although while 50-NS3-TRCA-WCP30* exposed to sea water for an duration of 148 days, the crystals identified are $CaSi_2O_5{\cdot}2H_2O$ in the form of calcium silicate hydrate (CSH) (Ref-00–011-0595), Na ($AlSi_3O_8$) in the form of albite (SAS) (Ref-01–076-0898), Ca $(OH)_2$ in the form of calcium hydroxide (CH) (Ref-01–084-1267), $CaCO_3$ in the form of aragonite (Ref-00–003-0893), and SiO_2 in the form of quartz (Q) (Ref-01–083-2468). It is evident that low intensity was identified with regard to CSH peaks as compared to water cured 28 aged samples. It confirms that crystalline nature of CSH gels deteriorated due abrasive contact of reactive salts. Overall, its resulted information of SAS in the form of albite and this additional formation exhibits microstructural pressure on concrete resulting in leaching of reactive salts [55, 56, 58–60, 80, 81]. These findings are in line with reduction in compressive strength and weight loss observations (refer to Section 6.2) and it is even confirmed through FE-SEM, EDS, FTIR, and quality characterizations.

7.4 FTIR

FTIR bands are exhibited as in Fig. 23 for ternary paste bonded adhered mortar of 50-NS3-TRCA-WCP30* cases after 28-day water curing, 148-day HCL exposure, and 148 days to sea water exposure conditions. FTIR bands are in line with the findings of XRD, FE-SEM, and EDS. Table 10 confirms the identification for group and compounds of ternary paste bonded adhered mortar and supported with the literuture. Si–O stretching band (ν) appears at 1029–1023 cm^{-1} which confirms the CSH vibrations. Identification of stretching at 1077 cm^{-1} and 1081 cm^{-1} represents polymerization of the orthosilicate units ($Sio^{4-}{}_4$) due to HCL and sea water exposure conditions in associate with formation of SAS. It indicates that these are As^{5+} impregnated samples which impart detoriation of CSH crystals and As^{5+} are not a good oxidising agent resulting in instability of mortar [96]. Further in confidance with XRD and FTIR

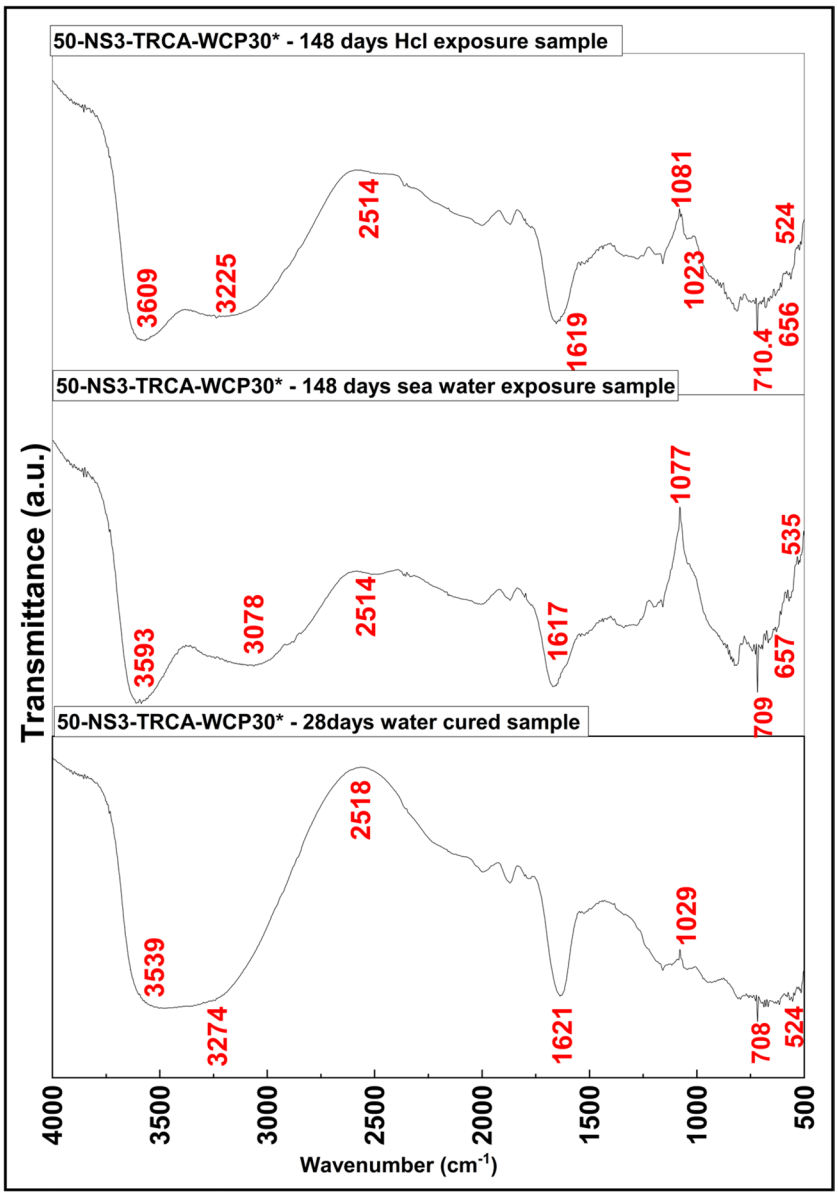

Fig. 23 FTIR analysis of ternary binding paste-based adhered mortar of 50-NS3-TRCA-WCP30*

Table 10 Identification for group and compounds of ternary paste bonded adhered mortar of 50-NS3-TRCA-WCP30*

(cm^{-1})	Group	Compounds	References
3609–3078	H_2O, OH, hydrogen bonds	Gypsum	[89–93]
2518–2514	ν C-O (harmonic bands)	Calcite, $CaCO_3$	[89–93]
1621–1619	H_2O, ν O–H	H_2O	[89–92]
1029–1023	ν Si–O	CSH vibrations	[89, 90, 92, 94]
1080–1011	Polymerized silica	CSH, SAS vibrations	[90–95]
708–710.4	ν C-O	Calcite, $CaCO_3$	[89–93]
656–658	ν SiO_4	Quartz, silica	[89, 91–95]
524, 535	ν Ca–Cl	$CaCl_2{\cdot}2H_2O$	[89–93]

findings, in composites after exposure to wild conditions (HCL and sea water), trace of ν Ca–Cl stretching confirms the identification of CC at 524 cm^{-1} and 535 cm^{-1} in low quantity due to its more solubility characteristics. Identification of gypsum compound associated with H_2O, OH, and hydrogen bonds at 3609 to 3078 cm^{-1} confirms the exposure

reaction with wild conditions. Overall, these findings are in line with loss percentage of compressive strength and weigth loss of respective concrete mixtures as discussed in Section 6.

8 Conclusions

From the present study, it is revealed that the recycled concrete aggregate may outperform natural aggregate through novel nano-silica prioritized-steam treatment technique and is also supported through WCP-based ternary pastes.

- 50% adhered mortar-based recycled concrete aggregate benefited more favourably from soaking with 3% nano-silica solution followed by a 3-h steam treatment.
- Mechanical characteristics such as compressive, split tensile, flexural, and elastic modulus revealed that 50-NS3-TRCA-WCP30* was the best performing mixture.
- A benefit of 50-NS3-TRCA-WCP30* over OPC-based CM in acid environments is that it degrades more slowly and exhibits better resilience due to low lime concentration in ternary binders' mixtures.
- UPV results are significantly proportional and in line with density, water absorption, mechanical, and also microstructure characterization of concrete and it found by R^2 varied from 0.88 to 0.98.
- Regarding UTRCA while expose to HCL, the presence of too much adhered mortar accelerates the degradation process by causing CSH decalcification and gypsum generation, which produces volume instability leading to reduction in weight and compressive strength of concrete.
- Compared to samples exposed to sea water, those exposed to HCL showed more robust decalcification of CSH rather than those exposed to sea water conditions because nano-silica inclusion in TRCA restricted the salt percolation resulting in more resistivity.
- FTIR, XRD, FE-SEM, and EDS are in line with the mechanical, durability, and quality performances of respective concrete mixes and it signifies the importance of bonding characteristics of concrete composites owing to the formation of additional CSH gels while 30% WCP incorporation made in ternary binder followed bonded with 3% NS-treated RCA.

It can be concluded from the above points that it is possible to replace 100% of recycled concrete aggregate with proposed novel treatment technique and with the support of 30% WCP-based ternary binder is possible to perform as an equant to natural aggregates by procuring same performance in concrete as its equant to conventional concrete with regard to all aspects.

Note: Regards All tests were conducted using three replicas, and the findings were afterwards displayed in a graph. The average value of the three replicas was used, and the range of variation was between 5 and 8%

Acknowledgements The authors are thankful to the Department of Civil Engineering, Manipal Institute of Technology, MAHE, Manipal, Karnataka, India. The authors also express gratitude to Dr. Murari M S, Scientific Officer, DSTPURSE Program, Mangalore University, who facilitated us to perform FESEM and EDS. Also, extend our thanks to the department of chemical engineering and DAMP Manipal Institute of Technology for TGA, FTIR, and XRD facilities.

Author contribution Dr A.U Rao and Dr Adithya Tantri: conceptualization, methodology, formal analysis, investigation, writing—original draft, validation, visualization, project administration, data curation, writing—review and editing. Prathibha P Shetty: methodology, resources, validation, project administration, writing—review and editing. Radhika Bhandary P: validation, visualization, investigation, data curation, writing—review and editing. Mr. Blesson S and Dr. Subhash C. Yaragal: data analysis, resources, validation, writing—review and editing.

Funding Open access funding provided by Manipal Academy of Higher Education, Manipal

Declarations

Competing interests The authors declare no competing interests.

References

1. Review technology news markets Ceramic World, (n.d.). https://issuu.com/tiledizioni/docs/cwr_india_2022
2. Indian CeramICs Industry, (n.d.)
3. R.P. Gupta, B. Biswas, Trends and growth in ceramics industry: a comparative study between India and China, n.d.
4. R.M. Senthamarai, P. Devadas Manoharan, Concrete with ceramic waste aggregate. Cem. Concr. Compos. **27**, 910–913 (2005). https://doi.org/10.1016/j.cemconcomp.2005.04.003
5. P.O. Awoyera, J.M. Ndambuki, J.O. Akinmusuru, D.O. Omole, Characterization of ceramic waste aggregate concrete. HBRC. J. **14**, 282–287 (2018). https://doi.org/10.1016/j.hbrcj.2016.11.003
6. D.M. Kannan, S.H. Aboubakr, A.D. EL-Dieb, M.M. Reda Taha, High performance concrete incorporating ceramic waste powder as large partial replacement of Portland cement. Constr. Build. Mater. **144**, 35–41 (2017). https://doi.org/10.1016/j.conbuildmat.2017.03.115

7. A. Heidari, D. Tavakoli, A study of the mechanical properties of ground ceramic powder concrete incorporating nano-SiO2 particles. Constr. Build. Mater. **38**, 255–264 (2013). https://doi.org/10.1016/j.conbuildmat.2012.07.110
8. A.S. El-Dieb, M.R. Taha, D. Kanaan, S.T. Aly, Ceramic waste powder: from landfill to sustainable concretes. Proc Instit. Civil Eng. Const. Mater. **171**, 109–116 (2018). https://doi.org/10.1680/jcoma.17.00019
9. V.L. Jerônimo, G.R. Meira, L.C.P. da Silva Filho, Performance of self-compacting concretes with wastes from heavy ceramic industry against corrosion by chlorides. Constr. Build. Mater. **169**, 900–910 (2018). https://doi.org/10.1016/j.conbuildmat.2018.03.034
10. P. Torkittikul, A. Chaipanich, Utilization of ceramic waste as fine aggregate within Portland cement and fly ash concretes. Cem. Concr. Compos. **32**, 440–449 (2010). https://doi.org/10.1016/j.cemconcomp.2010.02.004
11. F. Pacheco-Torgal, S. Jalali, Reusing ceramic wastes in concrete. Constr. Build. Mater. **24**, 832–838 (2010). https://doi.org/10.1016/j.conbuildmat.2009.10.023
12. S. Saeed Qadir, Strength and behavior of self-compacting concrete with crushed ceramic tiles as a partial replacement for coarse aggregate and subjected to elevated temperature. Int J Eng Techn Manag Appl Sci (IJETMAS) **3**(4), 278–286 (2015)
13. K. Rashid, A. Razzaq, M. Ahmad, T. Rashid, S. Tariq, Experimental and analytical selection of sustainable recycled concrete with ceramic waste aggregate. Constr. Build. Mater. **154**, 829–840 (2017). https://doi.org/10.1016/j.conbuildmat.2017.07.219
14. R. Senthamarai, P.D. Manoharan, D. Gobinath, Concrete made from ceramic industry waste: durability properties. Constr. Build. Mater. **25**, 2413–2419 (2011). https://doi.org/10.1016/j.conbuildmat.2010.11.049
15. M.C.S. Nepomuceno, R.A.S. Isidoro, J.P.G. Catarino, Mechanical performance evaluation of concrete made with recycled ceramic coarse aggregates from industrial brick waste. Constr. Build. Mater. **165**, 284–294 (2018). https://doi.org/10.1016/j.conbuildmat.2018.01.052
16. B. Zegardło, M. Szeląg, P. Ogrodnik, Ultra-high strength concrete made with recycled aggregate from sanitary ceramic wastes – the method of production and the interfacial transition zone. Constr. Build. Mater. **122**, 736–742 (2016). https://doi.org/10.1016/j.conbuildmat.2016.06.112
17. A. Halicka, P. Ogrodnik, B. Zegardlo, Using ceramic sanitary ware waste as concrete aggregate. Constr. Build. Mater. **48**, 295–305 (2013). https://doi.org/10.1016/j.conbuildmat.2013.06.063
18. Y Hong Cheng, F Huang, R Liu, J Long Hou, G Lu Li, Test research on effects of waste ceramic polishing powder on the permeability resistance of concrete. Mater. Struct. Mater. Const. 49 729–738 (2016) https://doi.org/10.1617/s11527-015-0533-6
19. A.M. Pitarch, L. Reig, A.E. Tomás, F.J. López, Effect of tiles, bricks and ceramic sanitary-ware recycled aggregates on structural concrete properties. Waste. Biomass. Valoriz. **10**, 1779–1793 (2019). https://doi.org/10.1007/s12649-017-0154-0
20. E. Vejmelková, M. Keppert, P. Rovnaníková, M. Ondráček, Z. Keršner, R. Černý, Properties of high performance concrete containing fine-ground ceramics as supplementary cementitious material. Cem. Concr. Compos. **34**, 55–61 (2012). https://doi.org/10.1016/j.cemconcomp.2011.09.018
21. L. Reig, M.M. Tashima, L. Soriano, M.V. Borrachero, J. Monzó, J. Payá, Alkaline activation of ceramic waste materials. Waste Biomass Valorization. **4**, 729–736 (2013). https://doi.org/10.1007/s12649-013-9197-z
22. H. Higashiyama, F. Yagishita, M. Sano, O. Takahashi, Compressive strength and resistance to chloride penetration of mortars using ceramic waste as fine aggregate. Constr. Build. Mater. **26**, 96–101 (2012). https://doi.org/10.1016/j.conbuildmat.2011.05.008
23. D.G. Nair, A. Fraaij, A.A.K. Klaassen, A.P.M. Kentgens, A structural investigation relating to the pozzolanic activity of rice husk ashes. Cem. Concr. Res. **38**, 861–869 (2008). https://doi.org/10.1016/j.cemconres.2007.10.004
24. S. Ray, M. Haque, S.A. Soumic, A.F. Mita, M.M. Rahman, B.B. Tanmoy, Use of ceramic wastes as aggregates in concrete production: a review,.J Build. Eng. 43 (2021). https://doi.org/10.1016/j.jobe.2021.102567.
25. R.V. Meena, J.K. Jain, H.S. Chouhan, A.S. Beniwal, Use of waste ceramics to produce sustainable concrete: a review, Clean Mater. 4 (2022). https://doi.org/10.1016/j.clema.2022.100085.
26. M. Kara, S.T. Yildirim, Y. Tabak, M. Kara, E. Günay, S.T. Yildirim, Ş. Yilmaz°, Ceramic tile waste as a waste management solution for concrete, n.d. https://www.researchgate.net/publication/297045994.
27. G.F. Huseien, A.R.M. Sam, K.W. Shah, J. Mirza, M.M. Tahir, Evaluation of alkali-activated mortars containing high volume waste ceramic powder and fly ash replacing GBFS. Constr. Build. Mater. **210**, 78–92 (2019). https://doi.org/10.1016/j.conbuildmat.2019.03.194
28. S Siddique T Gupta AA Thakare V Gupta S Chaudhary 2021 Acid resistance of fine bone china ceramic aggregate concrete, Euro. J. Environ. Civil. Eng. 25 1219 1232 https://doi.org/10.1080/19648189.2019.1572543
29. R. A U, R. Bhandary, M. B S, A. Tantri, S. Shenoy, M. Kamath, R.S. Shetty, Performance evaluation of hybrid glass wastes incorporated concrete, Engineered Science. 20 (2022). https://doi.org/10.30919/es8e758.
30. A Shenoy G Nayak A Tantri KK Shetty 2022 Materials Today : Proceedings Thermal transmission characteristics of plastic optical fibre embedded light transmitting concrete Mater Today Proc. https://doi.org/10.1016/j.matpr.2022.04.798
31. A Tantri G Nayak A Shenoy KK Shetty 2021 Development of self-compacting concrete using Bailey aggregate grading technique in comparison with Indian standard code of practice, Journal of Engineering Design and Technology. https://doi.org/10.1108/JEDT-02-2021-0095
32. S.V. Patil, K. Balakrishna Rao, G. Nayak, Quality improvement of recycled aggregate concrete using six sigma DMAIC methodology. Int. J. Math. Eng. Manag. Sci. 5 1409–1419 (2020) https://doi.org/10.33889/IJMEMS.2020.5.6.104
33. S.V. Patil, K.B. Rao, G. Nayak, Influence of silica fume on mechanical properties and microhardness of interfacial transition zone of different recycled aggregate concretes, Adv Civ Eng Mater. 10 (2021). https://doi.org/10.1520/ACEM20210011.
34. A Tantri G Nayak A Shenoy KK Shetty J Achar 2022 Implementation assessment of calcined and uncalcined cashew nut - shell ash with total recycled concrete aggregate in self - compacting concrete employing Bailey grading technique Springer International Publishing https://doi.org/10.1007/s41062-022-00907-8
35. E. Güneyisi, M. Gesoğlu, Z. Algin, H. Yazici, Effect of surface treatment methods on the properties of self-compacting concrete with recycled aggregates. Constr. Build. Mater. **64**, 172–183 (2014). https://doi.org/10.1016/j.conbuildmat.2014.04.090
36. A.S. Alqarni, H. Abbas, K.M. Al-Shwikh, Y.A. Al-Salloum, Treatment of recycled concrete aggregate to enhance concrete performance, Constr Build Mater. 307 (2021). https://doi.org/10.1016/j.conbuildmat.2021.124960.
37. H. Liu, X. Zhu, P. Zhu, C. Chen, X. Wang, W. Yang, M. Zong, Carbonation treatment to repair the damage of repeatedly recycled coarse aggregate from recycled concrete suffering from coupling action of high stress and freeze-thaw cycles, Constr Build Mater. 349 (2022). https://doi.org/10.1016/j.conbuildmat.2022.128688.
38. X. Wang, G. Du, L. Cai, J. Ren, W. Wang, Effect of crystallizer treatment on chloride diffusion and microstructure of recycled

aggregate concrete, Constr. Build. Mater. 321 (2022). https://doi.org/10.1016/j.conbuildmat.2021.126273.
39. L. Li, D. Xuan, A.O. Sojobi, S. Liu, C.S. Poon, Efficiencies of carbonation and nano silica treatment methods in enhancing the performance of recycled aggregate concrete, Constr. Build. Mater. 308 (2021). https://doi.org/10.1016/j.conbuildmat.2021.125080.
40. M.C. Rao, S.K. Bhattacharyya, S.V. Barai, Interfacial transition zone, strength and chloride penetration of recycled aggregate concrete. Ind. Conc. J. **89**, 54–65 (2015)
41. S Ray M Haque T Ahmed TT Nahin 2021 Comparison of artificial neural network (ANN) and response surface methodology (RSM) in predicting the compressive and splitting tensile strength of concrete prepared with glass waste and tin (Sn) can fiber J. King. Saud. Univ. Eng. Sci. https://doi.org/10.1016/j.jksues.2021.03.006
42. N.K. Bui, T. Satomi, H. Takahashi, Effect of mineral admixtures on properties of recycled aggregate concrete at high temperature. Constr. Build. Mater. **184**, 361–373 (2018). https://doi.org/10.1016/j.conbuildmat.2018.06.237
43. O. Çakir, Experimental analysis of properties of recycled coarse aggregate (RCA) concrete with mineral additives. Constr. Build. Mater. **68**, 17–25 (2014). https://doi.org/10.1016/j.conbuildmat.2014.06.032
44. S.M.S. Kazmi, M.J. Munir, Y.F. Wu, I. Patnaikuni, Y. Zhou, F. Xing, Influence of different treatment methods on the mechanical behavior of recycled aggregate concrete: a comparative study, Cem Concr Compos. 104 (2019). https://doi.org/10.1016/j.cemconcomp.2019.103398.
45. F. Kazemian, H. Rooholamini, A. Hassani, Mechanical and fracture properties of concrete containing treated and untreated recycled concrete aggregates. Constr. Build. Mater. **209**, 690–700 (2019). https://doi.org/10.1016/j.conbuildmat.2019.03.179
46. L. Li, D. Xuan, S.H. Chu, J.X. Lu, C.S. Poon, Efficiency and mechanism of nano-silica pre-spraying treatment in performance enhancement of recycled aggregate concrete, Constr. Build. Mater. 301 (2021). https://doi.org/10.1016/j.conbuildmat.2021.124093.
47. L.P. Singh, S.R. Karade, S.K. Bhattacharyya, M.M. Yousuf, S. Ahalawat, Beneficial role of nanosilica in cement based materials - a review. Constr. Build. Mater. **47**, 1069–1077 (2013). https://doi.org/10.1016/j.conbuildmat.2013.05.052
48. O.R. Kavitha, V.M. Shanthi, G.P. Arulraj, V.R. Sivakumar, Applied Clay Science Microstructural studies on eco-friendly and durable self-compacting concrete blended with metakaolin. Appl. Clay Sci. **124–125**, 143–149 (2016). https://doi.org/10.1016/j.clay.2016.02.011
49. H. Siad, H.A. Mesbah, H. Khelafi, S. Kamali-Bernard, M. Mouli, Effect of mineral admixture on resistance to sulphuric and hydrochloric acid attacks in selfcompacting concrete. Can. J. Civ. Eng. **37**, 441–449 (2010). https://doi.org/10.1139/L09-157
50. Z. Shi, Z. Shui, Q. Li, H. Geng, Combined effect of metakaolin and sea water on performance and microstructures of concrete. Constr. Build. Mater. **74**, 57–64 (2015). https://doi.org/10.1016/j.conbuildmat.2014.10.023
51. A. Karlsson, J. Ejlertsson, Addition of HCl as a means to improve biogas production from protein-rich food industry waste. Biochem. Eng. J. **61**, 43–48 (2012). https://doi.org/10.1016/j.bej.2011.12.003
52. E. Vincke, E. Van Wanseele, A. Beeldens, N. De Belie, L. Taerwe, V. Gemert, W. Verstraete, `, 2002. www.elsevier.com/locate/ibiod.
53. V. Marcos-Meson, G. Fischer, C. Edvardsen, T.L. Skovhus, A. Michel, Durability of steel fibre reinforced concrete (SFRC) exposed to acid attack – a literature review. Constr. Build. Mater. **200**, 490–501 (2019). https://doi.org/10.1016/j.conbuildmat.2018.12.051
54. C. Mariam Ninan, K.P. Ramaswamy, R. Sajeeb, A critical review on the factors influencing the design of test methods for assessing acid attack in concrete. Conf. Ser. Mater. Sci. Eng. 1114, 012013 (2021) https://doi.org/10.1088/1757-899x/1114/1/012013
55. K. De Weerdt, H. Justnes, M.R. Geiker, Changes in the phase assemblage of concrete exposed to sea water. Cem. Concr. Compos. **47**, 53–63 (2014). https://doi.org/10.1016/j.cemconcomp.2013.09.015
56. B. Benny, M. Bazli, A. Rajabipour, M. Arashpour, Durability of tubular sea water sea sand concrete and fibre-reinforced polymer hybrid structures: mechanisms and effective parameters: critical overview and discussion, Constr. Build. Mater. 366 (2023). https://doi.org/10.1016/j.conbuildmat.2022.130206.
57. M. Moinul Islam, M. Saiful Islam, M. Al-Amin, M. Mydul Islam, *Suitability of seawater on curing and compressive strength of structural concrete* (2012). https://www.jce-ieb.org/doc_file/4001004.pdf
58. T. Jena, K.C. Panda, Influence of sea water on strength and durability properties of concrete, in: Advances in Structural Engineering: Materials, Volume Three, Springer India, 2015: pp. 1863–1873. https://doi.org/10.1007/978-81-322-2187-6_143.
59. T. Li, X. Liu, Y. Zhang, H. Yang, Z. Zhi, L. Liu, W. Ma, S.P. Shah, W. Li, Preparation of sea water sea sand high performance concrete (SHPC) and serving performance study in marine environment, Constr. Build. Mater. 254 (2020). https://doi.org/10.1016/j.conbuildmat.2020.119114.
60. M. Moinul Islam, M. Islam, B. Chandra Mondal, M. Rafiqul Islam, *Strength behavior of concrete using slag with cement in sea water environment* (2010) https://www.jce-ieb.org/doc_file/3802004.pdf
61. M.M. El-Hawary, A. Abdul-Jaleel, Durability assessment of epoxy modified concrete. Constr. Build. Mater. **24**, 1523–1528 (2010). https://doi.org/10.1016/j.conbuildmat.2010.02.004
62. IS: 4031 (Part 6), Methods of physical tests for hydraulic cement part 6 determination of compressive strength of hydraulic cement other than masonry cement (First Revision), 2005. https://ia800400.us.archive.org/0/items/gov.in.is.4031.6.1988/is.4031.6.1988.pdf.
63. IS: 383 - 2016, *Coarse and fine aggregate for concrete* (2016) https://icikbc.org/docs/IS383-2016.pdf
64. B. of Indian Standards, IS 2386–4 (1963): Methods of test for aggregates for concrete, in *Part 4: Mechanical properties*. (n.d.). https://law.resource.org/pub/in/bis/S03/is.2386.4.1963.pdf
65. A. Mohammed, S. Rafiq, W. Mahmood, R. Noaman, K. Ghafor, W. Qadir, Q. Kadhum, Characterization and modeling the flow behavior and compression strength of the cement paste modified with silica nano-size at different temperature conditions. Constr. Build. Mater. **257**, 119590 (2020). https://doi.org/10.1016/j.conbuildmat.2020.119590
66. O.A. Naniz, M. Mazloom, E ff ects of colloidal nano-silica on fresh and hardened properties of self- compacting lightweight concrete. EJ. Build. Eng. **20**, 400–410 (2018). https://doi.org/10.1016/j.jobe.2018.08.014
67. N. Hani, O. Nawawy, K.S. Ragab, M. Kohail, The effect of different water/binder ratio and nano-silica dosage on the fresh and hardened properties of self-compacting concrete. Constr. Build. Mater. **165**, 504–513 (2018). https://doi.org/10.1016/j.conbuildmat.2018.01.045
68 A Tantri G Nayak M Kamath A Shenoy KK Shetty 2021 Utilization of cashew nut-shell ash as a cementitious material for the development of reclaimed asphalt pavement incorporated self compacting concrete Constr. Build. Mater. 301 124197 https://doi.org/10.1016/j.conbuildmat.2021.124197
69. B. of Indian Standards, *IS 10262 (2009): Guidelines for concrete mix design proportioning* (n.d.). https://law.resource.org/pub/in/bis/S03/is.10262.2009.pdf
70 BS, 1881 Part 122: 1983 Testing concrete-method for determination of water absorption, in *British Standard*, vol. 3, (2009),

pp.420–457. https://dl.azmanco.com/standards/BS/BS%201881-Part%20122-83.pdf
71. M.E. Gülşan, R. Alzeebaree, A.A. Rasheed, A. Niş, A.E. Kurtoğlu, Development of fly ash/slag based self-compacting geopolymer concrete using nano-silica and steel fiber. Constr. Build. Mater. **211**, 271–283 (2019). https://doi.org/10.1016/j.conbuildmat.2019.03.228
72. Y. Abadou, A. Ghrieb, R. Bustamante, H. Faid, Optimization by mixture design approach: impact of marble and ceramic recycle on properties of mortar based on air lime. J. Eng. Des. Technol. **18**, 1731–1747 (2020). https://doi.org/10.1108/JEDT-11-2019-0311
73. C.L. Hwang, M. Damtie Yehualaw, D.H. Vo, T.P. Huynh, Development of highstrength alkaliactivated pastes containing high volumes of waste brick and ceramic powders, Constr. Build. Mater. 218, 519–529 (2019). https://doi.org/10.1016/j.conbuildmat.2019.05.143
74. A. Jagadisha, K.B. Rao, G. Nayak, M. Kamath, Influence of nano-silica on the microstructural and mechanical properties of high-performance concrete of containing EAF aggregate and processed quarry dust. Constr. Build. Mater. **304**, 124392 (2021). https://doi.org/10.1016/j.conbuildmat.2021.124392
75. S.V. Patil, K.B. Rao, G. Nayak, Influence of silica fume on mechanical properties and microhardness of interfacial transition zone of different recycled aggregate concretes. Adv. Civ. Eng. Mater. **10**, 20210011 (2021). https://doi.org/10.1520/acem20210011
76. R. Sharma, R.A. Khan, Durability assessment of self compacting concrete incorporating copper slag as fine aggregates. Constr. Build. Mater. **155**, 617–629 (2017). https://doi.org/10.1016/j.conbuildmat.2017.08.074
77. N. Palankar, A.U. Ravi Shankar, B.M. Mithun, Durability studies on eco-friendly concrete mixes incorporating steel slag as coarse aggregates, J Clean Prod. 129, 437–448 (2016) . https://doi.org/10.1016/j.jclepro.2016.04.033.
78. T.G. Nijland, J.A. Larbi, Microscopic examination of deteriorated concrete, in: Non-Destructive Evaluation of Reinforced Concrete Structures: Deterioration Processes and Standard Test Methods, Elsevier Inc., 2010: pp. 137–179. https://doi.org/10.1533/9781845699536.2.137.
79. K.J. Rao, K. Keerthi, S. Vasam, Acid resistance of quaternary blended recycled aggregate concrete. Case Stud. Const. Mater. **8**, 423–433 (2018). https://doi.org/10.1016/j.cscm.2018.03.005
80. Z. Lu, G. Liu, Y. Wu, M. Dai, M. Jiang, J. Xie, Recycled aggregate seawater–sea sand concrete and its durability after immersion in seawater, J. Build. Eng. 65 (2023). https://doi.org/10.1016/j.jobe.2022.105780.
81. J. Xiao, K. Zhang, Q. Zhang, Strain rate effect on compressive stress–strain curves of recycled aggregate concrete with seawater and sea sand. Constr. Build. Mater. **300**, 124014 (2021). https://doi.org/10.1016/j.conbuildmat.2021.124014
82. R. Cheraghalizadeh, T. Akcaoglu, Utilization of olive waste ash and sea sand powder in self - compacting concrete, Iranian Journal of Science and Technology, Transactions of. Civ. Eng. **43**, 663–672 (2019). https://doi.org/10.1007/s40996-018-0224-y
83. W. Zhao, Z. Fan, X. Li, L. Kong, L. Zhang, Characterization and comparison of corrosion layer microstructure between cement mortar and alkali-activated fly ash/slag mortar exposed to sulfuric acid and acetic acid, Materials. 15 (2022). https://doi.org/10.3390/ma15041527.
84. M. Teymouri, K. Behfarnia, A. Shabani, Mix design effects on the durability of alkali-activated slag concrete in a hydrochloric acid environment, Sustainability (Switzerland). 13 (2021). https://doi.org/10.3390/su13148096.
85. S. Blesson, A.U. Rao, Agro-industrial-based wastes as supplementary cementitious or alkali-activated binder material: a comprehensive review, Innov. Infrast. Solut. 8 (2023). https://doi.org/10.1007/s41062-023-01096-8.
86. Q. Zhao, T. He, G. Zhang, Y. Li, G. Rong, Q. Ding, Influence of structural characterization of C3S-C3A paste under sulfate attack, Materials. 16 (2023). https://doi.org/10.3390/ma16010077.
87. A. Hendi, A. Behravan, D. Mostofinejad, A. Sedaghatdoost, M. Amini, A step towards green concrete: effect of waste silica powder usage under HCl attack. J. Clean. Prod. **188**, 278–289 (2018). https://doi.org/10.1016/j.jclepro.2018.03.288
88. R.E. Beddoe, Modelling acid attack on concrete: part II A computer model. Cem. Concr. Res. **88**, 20–35 (2016). https://doi.org/10.1016/j.cemconres.2015.10.012
89. A.S. Benosman, M. Mouli, H. Taibi, M. Belbachir, Y. Senhadji, I. Bahlouli, D. Houivet, Studies on chemical resistance of PET-mortar composites: microstructure and phase composition changes. Engineering **05**, 359–378 (2013). https://doi.org/10.4236/eng.2013.54049
90. M.A. Trezza, A.E. Lavat, Analysis of the system 3CaO·Al2O3-CaSO4·2H2O-CaCO3-H2O by FT-IR spectroscopy. Cem. Concr. Res. **31**, 869–872 (2001). https://doi.org/10.1016/S0008-8846(01)00502-6
91. R. Ylmén, U. Jäglid, B.M. Steenari, I. Panas, Early hydration and setting of Portland cement monitored by IR, SEM and Vicat techniques. Cem. Concr. Res. **39**, 433–439 (2009). https://doi.org/10.1016/j.cemconres.2009.01.017
92. J.T. Kloprogge, R.D. Schuiling, Z. Ding, L. Hickey, D. Wharton, R.L. Frost, Vibrational spectroscopic study of syngenite formed during the treatment of liquid manure with sulphuric acid. Vib. Spectrosc. **28**, 209–221 (2002). https://doi.org/10.1016/S0924-2031(01)00139-4
93. T.L. Hughes, C.M. Methven, T.G.J. Jones, S.E. Pelham, P. Fletcher, C. Hall, Determining cement composition by Fourier transform infrared spectroscopy. Adv. Cem. Based Mater. **2**, 91–104 (1995). https://doi.org/10.1016/1065-7355(94)00031-X
94. S.K. Pokharel, M.S. Setzer, S.E. Greenleaf, N.S. Dosoky, B.R. Jackes, W.N. Setzer, Structure of calcium silicate hydrate (C-S-H):near-, mid-, and far-infrared spectroscopy. Rec. Nat. Prod. **11**, 1–8 (2017)
95. J. Péra, S. Husson, B. Guilhot, Influence of finely ground limestone on cement hydration. Cem. Concr. Compos. **21**, 99–105 (1999). https://doi.org/10.1016/S0958-9465(98)00020-1
96. M.Y.A. Mollah, M. Kesmez, D.L. Cocke, An X-ray diffraction (XRD) and Fourier transform infrared spectroscopic (FT-IR) investigation of the long-term effect on the solidification/ stabilization (S/S) of arsenic(V) in Portland cement type-V. Sci. Total. Environ. **325**, 255–262 (2004). https://doi.org/10.1016/j.scitotenv.2003.09.012